Intelligent Adaptive Backstepping $\mathcal{H}_\infty$ Tracking Control System for a DSP-Based PMSM Servo Drive

Fayez F. M. El-Sousy, and Khaled A. Abuhasel

Abstract—This paper proposes an intelligent adaptive backstepping $\mathcal{H}_\infty$ tracking control system (IABHTCS) for the position control of permanent-magnet synchronous motor (PMSM) servo drive. The IABHTCS incorporates an ideal backstepping controller, a dynamic recurrent-fuzzy-wavelet-neural-network (DRFWNN) uncertainty observer and a robust $\mathcal{H}_\infty$ controller. First, a backstepping position controller is designed and analyzed to stabilize the PMSM servo drive system. However, particular information about the uncertainties of the PMSM servo drive is required in the ideal backstepping control law so that the corresponding control performance can not influenced seriously. To relax the requirement for the value of the lumped uncertainty in the backstepping controller , an adaptive DRFWNN uncertainty observer is designed to adaptively estimate the non-linear uncertainties online. In addition, the robust controller is designed to achieve $\mathcal{H}_\infty$ tracking performance to recover the residual of the approximation error and external disturbances with desired attenuation level. The online adaptive control laws are derived based on the Lyapunov stability analysis; the Taylor linearization technique and $\mathcal{H}_\infty$ control theory, so that the stability of the IABHTCS can be guaranteed. Finally, a computer simulation is developed and an experimental system is established to testify the effectiveness of the proposed IABHTCS. All control algorithms are implemented in a TMS320C31 DSP-based control computer. The simulation and experimental results confirm that the proposed IABHTCS can achieve favorable tracking performance regardless of parameters uncertainties by incorporating DRFWNN identifier, backstepping control and $\mathcal{H}_\infty$ control technique.

Keywords—Adaptive control, backstepping control, permanent-magnet synchronous motor (PMSM), dynamic recurrent-fuzzy-wavelet-neural-network (DRFWNN), Lyapunov stability theorem, $\mathcal{H}_\infty$ control.

I. INTRODUCTION

PERMENANT–MAGNET synchronous motor (PMSM) drives play a vitally important role in high-performance motion-control applications such as industrial robots and machine tools because of their compact size, high-power density, high air-gap flux density, high-torque/inertia ratio, high torque capability, high efficiency and free maintenance. The overall performance of a speed and/or position control of PMSM drives depend not only on the quickness and the precision of the system response, but also on the robustness of the control strategy which has been carried out to assure the same performances if exogenous disturbances and variations of the system parameters occur. In fact, the control of PMSM drives often necessitates the determination of the machine parameters. The online variations of parameters, which essentially depend on temperature variation, saturation and skin effects, external load disturbance and unmodeled dynamics in practical applications can affect the PMSM servo drive performances [1]–[3]. Therefore, to compensate for various uncertainties and nonlinearities, sophisticated control strategy is very important in PMSM servo drives. In practical applications, strong robustness to various uncertainties is always an important property that a good controller should achieve. From a practical point of view, complete information about uncertainties is difficult to acquire in advance. Therefore, the control performance of the PMSM servo drives may be seriously influenced. To deal with these uncertainties, much research has been carried out in recent years to apply various approaches to attenuate the effect of uncertainties. On the basic aspect, the conventional proportional-integral-derivative (PID) controllers are widely used in industry due to their simple control structure, ease of design and low cost [4]–[6]. On the other hand, the recently developed backstepping control technique is a powerful and systematic design methodology for AC motor servo drive systems, which offers a choice to accommodate the unmodeled and non-linear effects and parameter uncertainties. Numerous backstepping control design procedures have been proposed to control AC motor servo drive and nonlinear systems [7]–[20]. The key idea of the adaptive backstepping control design is to select recursively some appropriate functions of state variables as pseudo control inputs for lower dimension subsystems of the overall system. Each backstepping stage results in a new pseudo control design, expressed in terms of the pseudo control designs from preceding design stages. The procedure terminates a feedback design for the true control input, which achieves the original design objective by virtue of a final Lyapunov function, which is formed by summing the

Fyez F. M. El-Sousy is with the Department of Electrical Engineering, College of Engineering, Salman bin Abdulaziz University, Al-Kharj 11942, Saudi Arabia and on leave from Electronics Research Institute, Department of Power Electronics and Energy Conversion, Cairo 12622, Egypt. (phone: +966-54-386-1178; fax: +966-1-5453964; e-mail: f.elsousy@sau.edu.sa).

Khaled A. Abuhasel is with the Department of Mechanical Engineering, Salman bin Abdulaziz University, College of Engineering, Al-Kharj 11942, Saudi Arabia (e-mail: k.abuhasel@sau.edu.sa).

Lyapunov functions associated with each individual design stage. Thus, the backstepping control approach is capable of keeping the robustness properties with respect to the uncertainties [12]–[20].

As a result of rapid industrial developments, soft computing methodologies, such as fuzzy logic, neural network and wavelet, are getting more and more important. The concepts of fuzzy logic, wavelet technology and neural network have received a lot of attention in recent years [21]–[45], [69]–[76]. Intelligent control techniques in much research have been developed to improve the performance of PMSM servo drives and to deal with the nonlinearities and uncertainties using fuzzy logic, neural network, wavelet and/or the hybrid of them [21]–[26]. The concept of incorporating fuzzy logic into a neural network (NN) has grown into a popular research topic. In contrast to the pure neural network or fuzzy system, the fuzzy-neural-network (FNN) possesses both their advantages; it combines the capability of fuzzy reasoning in handling uncertain information and the capability of NNs in learning from the process [27]–[30]. On the other hand, the recurrent fuzzy-neural-network (RFNN), which naturally involves dynamic elements in the form of feedback connections used as internal memories, has been studied by some researchers in the past few years [31]–[35].

Wavelets have been combined with the neural network to create wavelet–neural–networks (WNNs). It combines the capability of artificial neural networks for learning from process together with the capability of wavelet decomposition [36]–[38] for identification and control of dynamic systems [39]–[45]. The training algorithms for WNN typically converge in a smaller number of iterations than the one used for conventional neural networks. Unlike the sigmoid functions used in the conventional neural networks, the second layer of WNN is a wavelet form, in which the translation and dilation parameters are included. Thus, WNN has been proved to be better than the other neural networks, since its structure can provide more potential to enrich the mapping relationship between inputs and outputs [37], [38]. There has been considerable interest in exploring the applications of WNN to deal with nonlinearities and uncertainties of real-time control systems. These WNN-based controllers combine the capability of NN for on-line learning ability and the capability of wavelet decomposition for identification ability. Thus, the WNN controllers have been adopted widely for the control of complex dynamical systems [36], [43]–[45], [47], [49].

In the last decade $\mathcal{H}_\infty$ optimal control theory has been well developed and found extensive application to efficiently treat robust stabilization and disturbance rejection problems [46]–[58]. In practical applications, strong robustness to various uncertainties is always an important property that a good controller should achieve. However, it is usually very difficult to get the complete information of uncertainties. Therefore, the control performance of the PMSM servo drives may be seriously influenced. From this point of view, $\mathcal{H}_\infty$ optimization synthesis is a very important and powerful tool for designing

robust controllers for PMSM servo drive systems. It can be successfully used to design controllers which give robust stability, low sensitivity to systems parameters variations, and to exogenous disturbances, and robust tracking property without steady-state error. In the last decade the approach of $\mathcal{H}_\infty$ optimal control has been widely discussed for robustness and its capability of disturbance attenuation in linear control systems [54], [55] and in nonlinear time-invariant control systems [46], [50]–[52].

A fuzzy wavelet neural network (FWNN) is combined wavelet theory with fuzzy logic and NN that can bring the low-level learning, good computational capability of the WNNs into fuzzy system and also high-level humanlike IF-THEN rule thinking reasoning of fuzzy system into the WNNs. The synthesis of a fuzzy wavelet neural inference system includes the determination of the optimal definitions of the premise and the consequent part of fuzzy IF–THEN rules. In recent years, FWNNs have been presented in some application areas [59]-[68]. The FWNNs consist of a set of rules and each rule contains a wavelet function in the consequent part of the rule. In [59], based on the theory of multiresolution of wavelet transforms and fuzzy concepts [67], FWNNs are proposed for approximation of an arbitrary nonlinear function. Through tuning the shape of the membership functions, the approximating capability of FWNNs [59] could be improved while not increasing the number of the wavelet bases. With the identification and control applications, some researchers [60]-[62], [64] presented the FWNNs structures that used the gradient descent method to update/tune network parameters including wavelet parameters and weights. In [63], adaptive controller-based FWNNs that have learning laws derived from the Lyapunov theorem is proposed. The training of FWNNs [63] requires a smaller number of iterations while the performance of controller can achieve the higher approximating accuracy than the NNs.

In this paper, an intelligent adaptive backstepping $\mathcal{H}_\infty$ control system using dynamic recurrent FWNN (DRFWNN) is proposed. The DRFWNN is the combination between the recurrent structure and the FWNN and it is applied to approximate the unknown dynamics of the PMSM servo drive system. In addition, a robust $\mathcal{H}_\infty$ controller is developed to deal with the uncertainties including the inevitable approximation errors, unknown disturbances of the PMSM servo drive system. The rest of this paper is organized as follows. Section II presents the field–oriented control (FOC) and dynamic analysis of PMSM servo drive. Both the problem formulation and the description of the high-precision adaptive backstepping control system of the PMSM servo drive are introduced. The design methodology for the backstepping controller and IABHTCS are given in Section III. Also, the design procedures and adaptive learning algorithms of the proposed IABHTCS and robust $\mathcal{H}_\infty$ controller are described in details in Section III. The validity of the design procedure and the robustness of the proposed controller are verified by means of computer simulation and experimental analysis. Control

algorithms have been developed in a control computer which is based on a TMS320C31 and TMS320P14 DSP DS1102 control board. The dynamic performance of the PMSM servo drive system has been studied under load changes and parameter uncertainties. Numerical simulations and experimental results are provided to validate the effectiveness of the proposed control system in Section IV. Conclusions are introduced in Section V.

II. PMSM MODEL DESCRIPTION AND DYNAMIC ANALYSIS

The voltage equations of the stator windings in the rotating reference frame can be expressed in (1) and (2). Then, using FOC and setting d-axis current as zero, the electromagnetic torque is obtained as given in (3) and (4) [3]. The parameters of the surface-mounted PMSM are listed in Table I.

$$V_{qs}^r = R_s i_{qs}^r + L_{ss} \frac{d}{dt} i_{qs}^r + \omega_r L_{ss} i_{ds}^r + \omega_r \lambda_m' \qquad (1)$$

$$V_{ds}^r = R_s i_{ds}^r + L_{ss} \frac{d}{dt} i_{ds}^r - \omega_r L_{ss} i_{qs}^r \qquad (2)$$

The electromagnetic torque can be expressed as:

$$T_e = (3/2) \cdot (P/2) \cdot \lambda_m i_{qs}^r = K_t i_{qs}^r \qquad (3)$$

The mechanical equation can be expressed as:

$$T_e = J_m \left(\frac{2}{P}\right) \frac{d^2}{dt^2} \theta_r + \beta_m \left(\frac{2}{P}\right) \frac{d}{dt} \theta_r + T_L \qquad (4)$$

From (3) and (4), the mechanical dynamics is simplified as:

$$\ddot{\theta}_r = -\frac{\beta_m}{J_m} \left(\frac{2}{P}\right) \dot{\theta}_r + \frac{K_t}{J_m} \left(\frac{2}{P}\right) i_{qs}^{r*} - \left(\frac{2}{P}\right) \frac{1}{J_m} T_L \qquad (5)$$

$$\ddot{\theta}_r = A_m \dot{\theta}_r + B_m U(t) + D_m T_L \qquad (6)$$

where $A_m = -(\beta_m / J_m)(P/2)$, $B_m = (K_t / J_m)(P/2)$, $D_m = -(P/2)(1/J_m)$, $U(t) = i_{qs}^{e*}(t)$ is the control effort and $K_t = (3/2)(P/2)\lambda_m$.

Now, assume that the parameters of the PMSM are well known and the external load disturbance is absent, rewriting (6) can represent the model of the PMSM servo drive system.

$$\ddot{\theta}_r(t) = A_m \dot{\theta}_r(t) + B_m U(t) \qquad (7)$$

By considering the dynamics in (6) with parameter variations, load disturbance and unpredictable uncertainties will give:

$$\ddot{\theta}_r(t) = (A_n + \Delta A_m)\dot{\theta}_r(t) + (B_n + \Delta B_m)U(t) \\ + (D_n + \Delta D_m).T_L \qquad (8)$$

$$\ddot{\theta}_r(t) = A_n \dot{\theta}_r(t) + B_n[U(t) + \Gamma(t)] \qquad (9)$$

where A_n, B_n and D_n are the nominal parameters of A_m, B_m and D_m respectively. ΔA_m, ΔB_m, ΔD_m and T_L are the uncertainties due to mechanical parameters J_m and β_m, and $\Gamma(t)$ is the lumped parameter uncertainty (PU) and is defined as:

$$\Gamma(t) = \Delta A_m \dot{\theta}_r(t) + \Delta B_m U(t) + (D_n + \Delta D_m)T_L \qquad (10)$$

III. INTELLIGENT ADAPTIVE BACKSTEPPING $\mathcal{H}_\infty$ TRACKING CONTROL SYSTEM (IABHTCS)

In this section, the problem formulation, analysis and design

of the ideal backstepping controller (IBC) and the IABHTCS for the PMSM servo drive are introduced. Although the desired tracking and regulation position control performance can be realized using the IBC at the nominal PMSM parameters, the performance of the servo drive system still sensitive to parameter variations. To solve this problem and in order to control the rotor position of the PMSM effectively, an IABHTCS is proposed. The configuration of the proposed control scheme, which combines an IBC, a DRFWNN uncertainty observer and a robust $\mathcal{H}_\infty$ controller, for PMSM servo drive is shown in Fig.1. The hybrid control law is assumed to take the following form:

$$U_{qs}^*(t) = i_{qs}^{r*}(t) = U_{qs}^{IBC}(t) + U_{qs}^{RFWNNC}(t) + U_{qs}^{RC}(t) \qquad (11)$$

where $U_{qs}^{IBC}(t)$ is ideal backstepping controller, $U_{qs}^{RFWNNC}(t)$ is the DRFWNN uncertainty observer and $U_{qs}^{RC}(t)$ is the robust $\mathcal{H}_\infty$ tracking controller. The adaptive backstepping controller is used as the main tracking controller in which the DRFWNN uncertainty observer is used to adaptively estimate the non-linear uncertainties $\Gamma(t)$ online, while the robust $\mathcal{H}_\infty$ controller is designed to recover the residual of the approximation error and external disturbances with desired attenuation level.

TABLE I PARAMETERS OF PMSM

Quantity	Symbol	Value
Nominal power	P_n	1 hp (3-phase)
Stator self inductance	L_{ss}	0.05 H
Stator resistance	R_s	1.5 Ω
Voltage constant	λ_m	0.314 V.s/rad
Number of poles	P	4
Rotor inertia	J_m	0.003 kg.m^2
Friction coefficient	β_m	0.0009 N.m/rad/sec
Nominal speed (electrical)	ω_r	377 rad/sec
Rated torque	T_e	3.6 N.m
Rated current	I	4 A
Rated voltage	V_{L-L}	208 V
Rated frequency	f	60 Hz
Torque constant	K_t	0.95 N.m/A
Encoder resolution	n	4×10000 p/r

A. Ideal Backstepping Controller (IBC)

The control objective is to design a suitable control law for the PMSM drive given by (1)-(9) so that the state trajectory of the rotor position $\theta_r(t)$ can track the desired position $\theta_r^m(t)$ trajectory asymptotically specified by the reference model despite the presence of unknown system dynamics and external load disturbance. Assume that $\theta_r^m(t)$, $\dot{\theta}_r^m(t)$ and $\ddot{\theta}_r^m(t)$ are all bounded functions of time. When all PMSM dynamics are well known, the design of the IBC is described step-by-step as follows:

Step 1: Define the tracking error state

$$e_1(t) = \theta_r(t) - \theta_r^m(t) \qquad (12)$$

Then, the derivative of the tracking error is:

$$\dot{e}_1(t) = \omega_r - \dot{\theta}_r^m(t) \qquad (13)$$
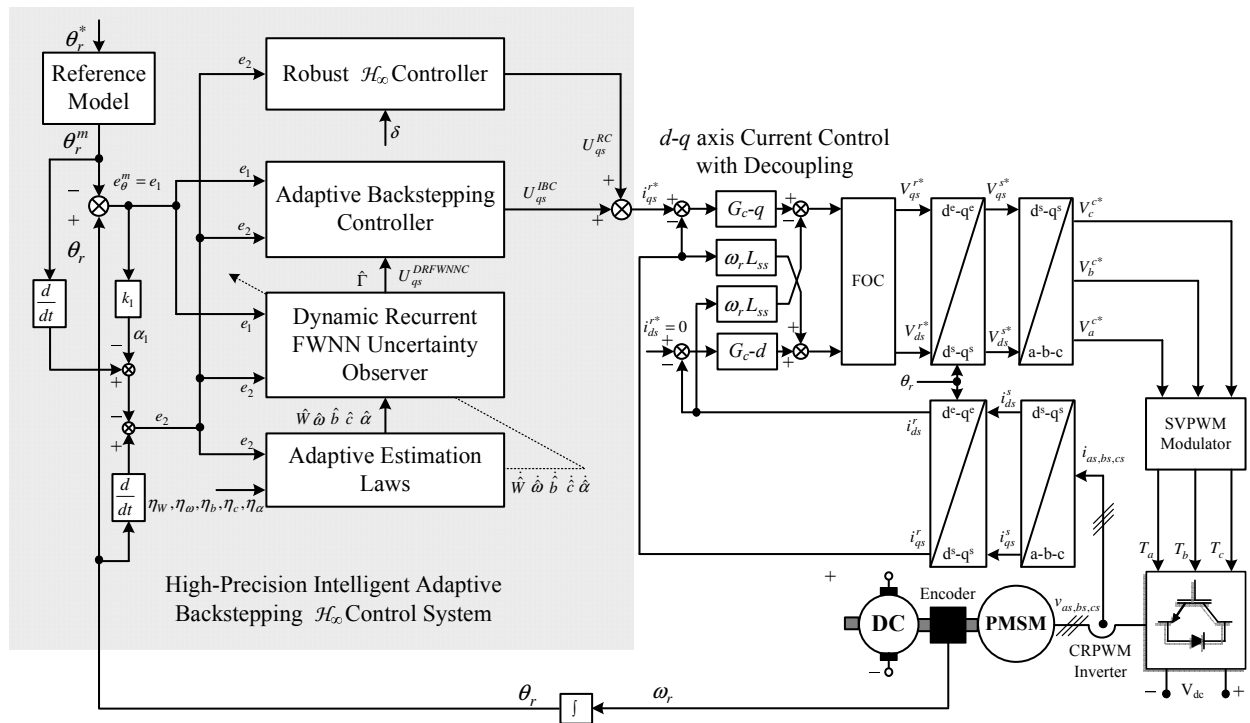
Fig. 1 Structure of the proposed intelligent adaptive backstepping $\mathcal{H}_\infty$ tracking control system (IABHTCS) for PMSM servo drive

where $\dot{\theta}_r(t) = \omega_r(t)$ can be viewed as virtual control in (13). Next, define the following stabilizing function [8]:

$$\alpha_1(t) = -k_1 e_1(t) + \dot{\theta}_r^m(t) \tag{14}$$

where k_1 is a positive constant. The Lyapunov function is chosen as

$$V_1(t) = \frac{1}{2} e_1^2(t) \tag{15}$$

Define the tracking error state

$$\begin{aligned} e_2(t) &= -\alpha_1(t) + \omega_r(t) \\ &= k_1 e_1(t) - \dot{\theta}_r^m(t) + \theta_r(t) \\ &= k_1 e_1(t) + \dot{e}_1(t) \end{aligned} \tag{16}$$

The derivative of $V_1(t)$ and using (13), (14) and (16)

$$\begin{aligned} \dot{V}_1(t) &= e_1(t)\dot{e}_1(t) \\ &= e_1(t)[-k_1 e_1(t) + e_2(t)] \\ &= -k_1 e_1^2(t) + e_1(t)e_2(t) \end{aligned} \tag{17}$$

Step 2: The derivative of the tracking error $e_2(t)$ and substituting (9):

$$\begin{aligned} \dot{e}_2(t) &= -\dot{\alpha}_1(t) + \dot{\omega}_r(t) \\ &= \ddot{e}_1(t) + k_1 \dot{e}_1(t) = -e_1(t) - k_2 e_2(t) \\ &= k_1 \dot{e}_1(t) - \ddot{\theta}_r^m(t) + A_{mn}\dot{\theta}_r(t) + B_{mn}U(t) + \Gamma(t) \end{aligned} \tag{18}$$

In order to design a controller including the tracking performance and the ability of rejecting external disturbance and parameters uncertainties, the related terms of $e_2(t)$ is added into (15) to obtain a new Lyapunov function

$$V_2(t) = V_1(t) + \frac{1}{2} e_2^2(t) \tag{19}$$

Then, the first derivative of $V_2(t)$ is taken and substituting (16), (17) and (18)

$$\begin{aligned} \dot{V}_2(t) &= \dot{V}_1(t) + e_2(t)\dot{e}_2(t) \\ &= -k_1 e_1^2(t) + e_1(t)e_2(t) \\ &\quad + e_2(t)\{k_1 \dot{e}_1(t) - \ddot{\theta}_r^m(t) + A_{mn}\dot{\theta}_r(t) + B_{mn}U(t) + \Gamma(t)\} \end{aligned} \tag{20}$$

Step 3: If the system dynamic function is known, the ideal backstepping controller can be obtained from (9), (18) as

$$\begin{aligned} U_{qs}^{IBC}(t) = &\ B_{mn}^{-1}[\ddot{\theta}_r^m(t) - A_{mn}\dot{\theta}_r(t) - \Gamma(t) \\ &- k_1 \dot{e}_1(t) - k_2 e_2(t) - e_1(t)] \end{aligned} \tag{21}$$

Step 4: Rewrite the derivative of the Lyapunov function (20) and substituting (21) will yield

$$\dot{V}_2(t) = -k_1 e_1^2(t) - k_2 e_2^2(t) \le 0 \tag{22}$$

Since $\dot{V}_2(t) \le 0$, $\dot{V}_2(t)$ is a negative semi-definite function (i.e. $V_2(t) \le V_2(0)$), which implies that $e_1(t)$ and $e_2(t)$ are bounded. Now define the following term:

$$Q(t) = k_1 e_1^2(t) + k_2 e_2^2(t) \le -\dot{V}_2(t) \tag{23}$$

Then

$$\int_0^t Q(\tau)d\tau \le V_2(0) - V_2(t) \tag{24}$$

Since $V_2(0)$ is bounded and $V_2(t)$ is non-increasing and bounded, the following result can be obtained:

$$\lim_{t \to \infty} \int_0^t Q(\tau)d\tau \le \infty \tag{25}$$

$$y_o^5 = U_{qs}^{*DRWFNNC} = \hat{\Gamma}$$
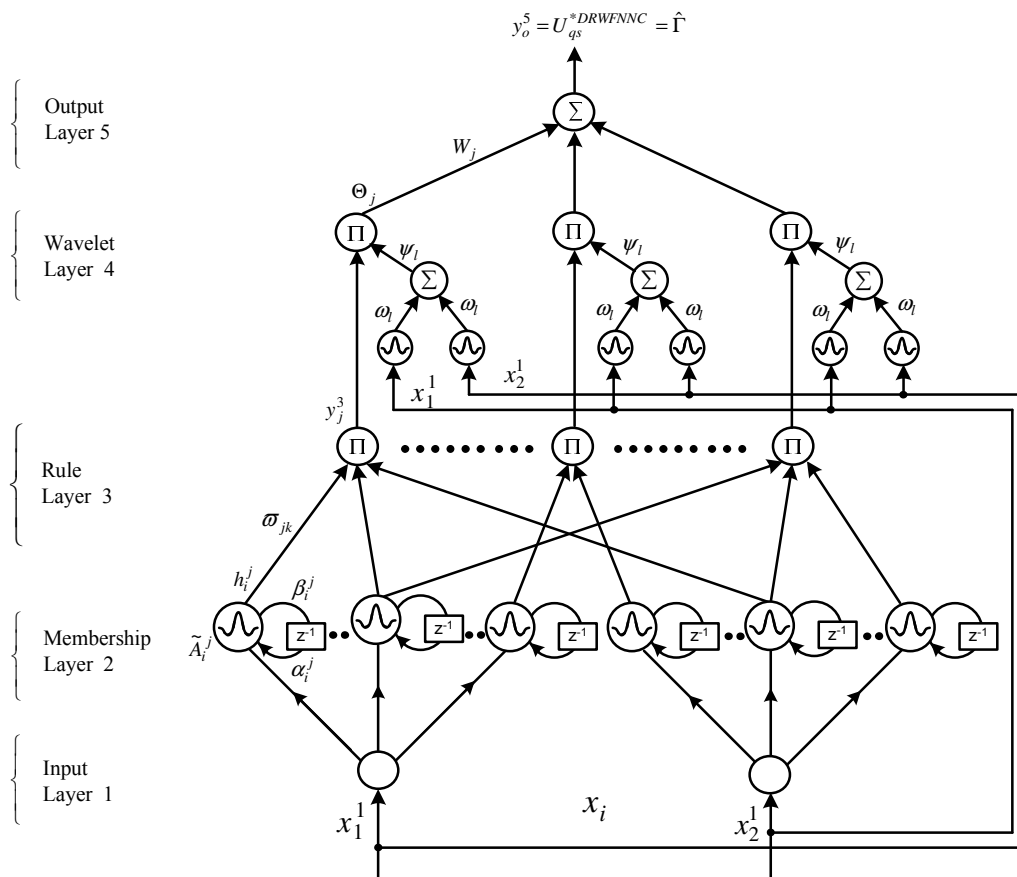
Fig. 2 Structure of five-layer DRFWNN

In addition, $\dot{Q}(t)$ is also bounded. Thus, $Q(t)$ is uniformly continuous. Using Barbalat's lemma [76]-[77], the following result can be obtained:

$$\lim_{t \to \infty} Q(t) = 0 \qquad (26)$$

This implies that $e_1(t)$ and $e_2(t)$ converge to zero as $t \to \infty$. As a result, the IBC in (21) will asymptotically stabilize the PMSM drive system.

Unfortunately, the parameter variations of the PMSM servo drive system are difficult to measure and the exact value of the external load disturbance is also difficult to know in advance for practical applications. Though, if the PMSM parameters are perturbed, the IBC specified by (21) can not be precisely obtained. Moreover, the stability of the PMSM servo drive may be destroyed. Therefore, to ensure the stability of the servo drive despite the existence of the uncertain dynamics and external load disturbance, a DRFWNN uncertainty observer is proposed to adapt the value of the lumped uncertainty, which is denoted $\hat{\Gamma}(t)$, online in the following section.

B. DRFWNN Uncertainty Observer

Dynamic recurrent neural network provides an effective way for the identification of dynamic systems. Through storing past state into delay units, networks have the memory capability. So, they can process the object related to time. The recurrent property is achieved in the proposed dynamic recurrent fuzzy wavelet neural network (DRFWNN). As a result, it not only

utilizes its previous knowledge, but also has better response for the dynamic systems. In this section the description of the DRFWNN is introduced. The DRFWNN combines the merits of the FNN, WNN and recurrent neural network. In addition, the appearance of the feedback loop with time-delay at the FWNN fuzzification layer will make RFWNN become a dynamic structure that has enough ability to deal with dynamics of PMSM servo drive system. The structure of the proposed DRFWNN is shown in Fig. 2. The wavelet-neural-network (WNN) is a nonlinear regression structure that represents input-output mappings by dilated and translated versions of wavelet function [68]. The output of the WNN is given by:

$$u_j = \sum_{j=1}^{k} \omega_j \psi_j(x_i) \qquad (27)$$

$$\psi_j(x_i) = |c_j|^{-\frac{1}{2}} \psi\left(\frac{x_i - b_j}{c_j}\right), \quad c_j \neq 0 \qquad (28)$$

where $\psi_j(x_i)$ represents the family of wavelets obtained from the single $\psi(x_i)$ function by translations and dilations, $b_j = \{b_{1j}, b_{2j}, \ldots, b_{nj}\}$ and $c_j = \{c_{1j}, c_{2j}, \ldots, c_{nj}\}$ are the translation and the dilation parameters, $\psi_j(x_i)$ is also the wavelet function of the jth unit of the hidden layer, ω_j are the weights between the hidden and output layers of the WNN, $x_i = \{x_1, x_2, \ldots, x_N\}$ are the input signals, b_j and c_j are the

translation and the dilation parameters of the wavelet function. The translation parameter determines the center position of the wavelet, whereas the dilation parameter controls the spread of the wavelet [36]-[42]. WNN has good generalization ability, can approximate complex function to some precession very compactly and can be easily trained than other network [39]. A good initialization of the parameters of the WNNs enables to obtain fast convergence. Different methods are proposed in the literature for the initialization of the wavelets such as orthogonal least square procedure [39]. An optimal choice of the translation and dilation parameters of the wavelet increases the training speed results in fast convergence. The approximation and convergence properties of the WNN are presented in [40]. Wavelet networks include wavelet functions in the neurons of the hidden layer of the network. The output of the WNN is calculated as

$$u_j = \sum_{j=1}^{k} \omega_j |c_j|^{-\frac{1}{2}} \exp\left(-\frac{1}{2}\left(\frac{x_i - b_j}{c_j}\right)^2\right) \qquad (29)$$

The structure of the DRFWNN is the combination of the recurrent structure and the FWNN. The basic concepts of FWNN, originally presented in [59]-[68], are briefly introduced. The FWNN combines Takagi-Sugeno-Kang (TSK) fuzzy system and the WNN. In a TSK fuzzy model, the domain interval of each input is separated into fuzzy regions and each region shows a membership function in the IF part of the fuzzy rules [61], [62]. A constant or a linear function of inputs is used in the THEN part of the rules. In this paper constant or linear functions in the THEN part of the rules are substituted with wavelet functions in order to increase the computational power of neuro-fuzzy system. The jth rule of the proposed DRFWNN is presented as follows:

R_j :

IF h_1^j is A_1^j and h_2^j is A_2^j ...and h_i^j is A_i^j ...and h_N^j is A_N^j

$$\text{THEN } y_o^5(n) = \sum_{j=1}^{M} y_j^4 \cdot W_j = \sum_{j=1}^{M} \Theta_j \cdot W_j \qquad (30)$$

where R_j is the jth rule; N is the number of input variables; $h_i^j(n) = x_i(n) + \beta_i^j(n-1)\alpha_i^j$, α_i^j represents the weight of the self-feedback loop, $\beta_i^j(n-1)$ indicates the output signal of the membership layer in the previous time, A_i^j is the linguistic term of the precondition part with wavelet membership function, W_j is the link weight output strength and y_o^5 is the output of the DRFWNN.

The Mexican Hat wavelet function $\psi(x) = (1 - x^2)\exp(-x^2/2)$ is used as the wavelet transform in this paper. The translated and dilated version of the Mexican Hat wavelet function is used, which is given by the following equation:

$$\psi\left(\frac{x_i - b_j}{c_j}\right) = \left(1 - \left(\frac{x_i - b_j}{c_j}\right)^2\right)\exp\left(-\frac{1}{2}\left(\frac{x_i - b_j}{c_j}\right)^2\right) \qquad (31)$$

The architecture of the proposed five-layer DRFWNN configuration is shown in Fig. 2, which comprises the input

layer (the i layer), membership and recurrent layer (the j layer), rule layer (the k layer), wavelet layer (the l layer) and output layer (the o layer). Moreover, z^{-1} represents a time-delay. The signal propagation and the basic function in each layer are introduced as follows.

1) Layer 1- Input Layer: The nodes in layer 1 transmit the input signals to the next layer. For every node i in the input layer, the net input and the net output can be represented as:

$$net_i^1(n) = x_i^1 \qquad (32)$$

$$y_i^1 = f_i^1(net_i^1(n)) = net_i^1(n) \quad i = 1, 2 \qquad (33)$$

where $x_1^1 = e_\theta^m(t)$, $x_2^1 = \dot{e}_\theta^m(t)$ and x_i^1 represents the ith input to the node of layer 1, n denotes the number of iterations.

2) Layer 2- Membership (Fuzzification) Layer: Each node in this layer performs a membership function. In this paper, the input of the membership layer can be represented by

$$h_i^j(n) = x_i(n) + \beta_i^j(n-1)\alpha_i^j \qquad (34)$$

where α_i^j represents the weight of the self-feedback loop, $\beta_i^j(n-1)$ indicates the output signal of layer 2 in the previous time and is defined with wavelet membership function as

$$\lambda_{A_i^j}(h_i^j) = -\exp\left(\frac{h_i^j - b_i^j}{c_i^j}\right)^2 \qquad (35)$$

$$net_j^2(h_i^j) = -\left(\frac{h_i^j - b_i^j}{c_i^j}\right)^2 \qquad (36)$$

$$y_j^2(n) = \beta_i^j[net_j^2(h_i^j)] = \exp[net_j^2(h_i^j)]$$

$$= \exp\left[-\left(\frac{h_i^j - b_i^j}{c_i^j}\right)^2\right] \qquad (37)$$

where $\exp[\cdot]$ is the exponential function, b_i^j and c_i^j ($i = 1,\ldots, n_i$; $j=1,\ldots, n_j$), respectively, are the translation and the dilation parameters of the wavelet function in the jth term of the ith input variable x_i to the node of this layer, n_j is the number of linguistic variables with respect to each input.

3) Layer 3- Rule Layer: Each node in this layer represents one fuzzy logic rule and performs precondition matching of a rule. Thus, the neuron in this layer is denoted by Π, which multiplies the incoming signals from layer 2 and outputs the product result, i.e., the firing strength of a rule. For the jth rule node:

$$net_j^3(n) = \prod_i^n \varpi_{jk}^3 y_j^2(n) \qquad (38)$$

$$y_j^3(n) = f_j^3(net_j^3(n)) = net_j^3(n)$$

$$= \prod_{i=1}^{n} \varpi_{jk}^3 y_j^2(n) = \prod_{i=1}^{n} \varpi_{jk}^3 \exp\left[-\left(\frac{h_i^j - b_i^j}{c_i^j}\right)^2\right] \qquad (39)$$

where x_j^3 represents the jth input to the node of layer 3; ϖ_{jk}^3 are the weights between the membership layer and the rule layer and are set to be equal to unity to simplify the

implementation for the real-time control; and n is the number of rules.

4) Layer 4- Wavelet Layer: The neuron in this layer multiplies the incoming signals, which are y_j^3 from the output of layer 3 (rule layer) and the output signal from the wavelet functions y_l.

The output of the lth wavelet is calculated as

$$y_l(h_i^j) = \psi_l(h_i^j) = \sum_{i=1}^{n} \omega_l |c_j|^{-\frac{1}{2}} \left(1 - \left(\frac{h_i^j - b_i^j}{c_i^j}\right)^2\right) \cdot \exp\left(-\frac{1}{2}\left(\frac{h_i^j - b_i^j}{c_i^j}\right)^2\right) \tag{40}$$

Furthermore, the process of this layer is described as follows:

$$net_j^4(n) = \prod_i^n y_l(h_i^j) \cdot y_j^3(n) \tag{41}$$

$$y_j^4(n) = f_j^4(net_j^4(n)) = net_j^4(n)$$
$$= \left(\prod_{i=1}^{n} \varpi_{jk}^3 \exp\left[-\left(\frac{h_i^j - b_i^j}{c_i^j}\right)^2\right]\right) \cdot$$
$$\sum_{i=1}^{n} \omega_l |c_j|^{-\frac{1}{2}} \left(1 - \left(\frac{h_i^j - b_i^j}{c_i^j}\right)^2\right) \cdot \exp\left(-\frac{1}{2}\left(\frac{h_i^j - b_i^j}{c_i^j}\right)^2\right) \tag{42}$$

5) Layer 5- Output Layer: The single node o in the output layer is denoted by Σ, which computes the overall output as the summation of all incoming signals. The final output of the DRFWNN, y_o^5, is calculated and the output node together with related links acts as a defuzzifier. The mathematical function is given by:

$$net_o^5(n) = \sum_{j=1}^{M} y_j^4 \cdot W_j \tag{43}$$

$$y_o^5(n) = f_o^5(net_o^5(n)) = net_o^5(n)$$
$$= \sum_{j=1}^{M} y_j^4 \cdot W_j = \sum_{j=1}^{M} \Theta_j \cdot W_j \tag{44}$$
$$= U_{qs}^{RFWNNC}(t) = \hat{\Gamma}$$

where the link weight W_j is the output strength and y_o^5 is the output of the DRFWNN controller and also is the estimated nonlinear function $\hat{\Gamma}$. Moreover, $y_o^5 = U_{qs}^{RFWNNC}(t) = \hat{\Gamma}$ for the uncertainty estimation of the PMSM servo drive; M is the number of rules and U_{qs}^{RFWNNC} is the control effort of the PMSM servo drive system.

The output of the DRWFNN identifier can be rewritten as

$$U_{qs}^{DRFWNNC}(E, W, \alpha, \omega, b, c) = W^T \Theta(E, \alpha, \omega, b, c) \tag{45}$$

where the tracking error vector E is the input of the DRFWNN, $W = [W_1, W_2, \ldots, W_M]^T$ in which W_j is initialized to be zero and adjusted during on-line operation;

$\Theta = [\Theta_1, \Theta_2, \ldots, \Theta_M]^T$ in which Θ_j is determined by the selected Mexican hat mother wavelet function; $\omega_j = [\omega_{1j}, \omega_{2j}, \ldots, \omega_{Mj}]^T$ are the weight coefficients between input and hidden layers; $b_j = [b_{1j}, b_{2j}, \ldots, b_{Mj}]^T$ are the translation parameters; $c_j = [c_{1j}, c_{2j}, \ldots, c_{Mj}]^T$ are the dilation parameters and $\alpha_j = [\alpha_{1j}, \alpha_{2j}, \ldots, \alpha_{Mj}]^T$ are the weights of self-feedback loops related to the hidden layer in the DRFWNN.

By the universal approximation theorem, there exists an ideal RFWNN identifier $U_{qs}^{*RFWNNC} = \Gamma^*$ such that [37]

$$\Gamma = \Gamma^* + \varepsilon = W^{*T}\Theta(E, \alpha^*, \omega^*, b^*, c^*) + \varepsilon \tag{46}$$

where ε is a minimum reconstructed error and assumed to be bounded by $|\varepsilon| \le \varepsilon^*$, in which ε^* is a positive constant; and α^*, ω^*, b^* and c^* are the optimal parameters of α, ω, b and c, respectively, in the DRFWNN. In fact, the optimal parameter vectors that are required to best approximate a given nonlinear function is defined as

$$\hat{\Gamma}(E, \hat{\alpha}, \hat{\omega}, \hat{b}, \hat{c}) = \hat{W}^T \hat{\Theta}(E, \hat{\alpha}, \hat{\omega}, \hat{b}, \hat{c}) \tag{47}$$

where $\hat{\alpha}$, $\hat{\omega}$, $\hat{b}$ and $\hat{c}$ are the estimation of α^*, ω^*, b^* and c^*, respectively. Subtracting (47) from (46), the approximation error, $\tilde{\Gamma}$, is defined as:

$$\tilde{\Gamma} = \Gamma - \hat{\Gamma} = \Gamma^* - \hat{\Gamma} + \varepsilon = W^{*T}\Theta^* - \hat{W}^T\hat{\Theta} + \varepsilon$$
$$= \tilde{W}^T\tilde{\Theta} + \hat{W}^T\tilde{\Theta} + \tilde{W}^T\hat{\Theta} + \varepsilon \tag{48}$$

where $\tilde{W} = (W^* - \hat{W})$ and $\tilde{\Theta} = (\Theta^* - \hat{\Theta})$. The weights of the DRFWNN are updated online to make its output approximate the unknown nonlinear function Γ accurately. To achieve this goal, the linearization technique is used to transform the nonlinear output of DRFWNN into partially linear form so that the Lyapunov theorem extension can be applied. The expansion of $\tilde{\Theta}$ in Taylor series is obtained as follows [30]:

$$\tilde{\Theta} = \begin{bmatrix} \tilde{\Theta}_1 \\ \tilde{\Theta}_2 \\ \vdots \\ \tilde{\Theta}_j \end{bmatrix} = \begin{bmatrix} \frac{\partial \Theta_1}{\partial \omega} \\ \frac{\partial \Theta_2}{\partial \omega} \\ \vdots \\ \frac{\partial \Theta_j}{\partial \omega} \end{bmatrix}^T_{\omega=\hat{\omega}} \tilde{\omega} + \begin{bmatrix} \frac{\partial \Theta_1}{\partial b} \\ \frac{\partial \Theta_2}{\partial b} \\ \vdots \\ \frac{\partial \Theta_j}{\partial b} \end{bmatrix}^T_{b=\hat{b}} \tilde{b} + \begin{bmatrix} \frac{\partial \Theta_1}{\partial c} \\ \frac{\partial \Theta_2}{\partial c} \\ \vdots \\ \frac{\partial \Theta_j}{\partial c} \end{bmatrix}^T_{c=\hat{c}} \tilde{c}$$
$$+ \begin{bmatrix} \frac{\partial \Theta_1}{\partial \alpha} \\ \frac{\partial \Theta_2}{\partial \alpha} \\ \vdots \\ \frac{\partial \Theta_j}{\partial \alpha} \end{bmatrix}^T_{\alpha=\hat{\alpha}} \tilde{\alpha} + g$$
$$\equiv \Theta_\omega^T \tilde{\omega} + \Theta_b^T \tilde{b} + \Theta_c^T \tilde{c} + \Theta_\alpha^T \tilde{\alpha} + g \tag{49}$$

(a) Experimental setup

(b) Block diagram of the proposed DSP-based control system

Fig. 3 DSP-based IABHTCS for PMSM servo drive

Rewriting (49), it can be obtained that

$$\tilde{\Theta} = A^T \tilde{\omega} + B^T \tilde{b} + C^T \tilde{c} + D^T \tilde{\alpha} + g \qquad (50)$$

where

$$A = \begin{bmatrix} (\partial \Theta_1 / \partial \omega) & (\partial \Theta_2 / \partial \omega) & \cdots & (\partial \Theta_j / \partial \omega) \end{bmatrix}^T \Big|_{\omega = \hat{\omega}},$$

$$B = \begin{bmatrix} (\partial \Theta_1 / \partial b) & (\partial \Theta_2 / \partial b) & \cdots & (\partial \Theta_j / \partial b) \end{bmatrix}^T \Big|_{b = \hat{b}},$$

$$C = \begin{bmatrix} (\partial \Theta_1 / \partial c) & (\partial \Theta_2 / \partial c) & \cdots & (\partial \Theta_j / \partial c) \end{bmatrix}^T \Big|_{c = \hat{c}},$$

$$D = \begin{bmatrix} (\partial \Theta_1 / \partial \alpha) & (\partial \Theta_2 / \partial \alpha) & \cdots & (\partial \Theta_j / \partial \alpha) \end{bmatrix}^T \Big|_{\alpha = \hat{\alpha}},$$

$\tilde{\omega} = (\omega^* - \hat{\omega})$, $\tilde{b} = (b^* - \hat{b})$, $\tilde{c} = (c^* - \hat{c})$, $\tilde{\alpha} = (\alpha^* - \hat{\alpha})$ and g is a vector of higher order terms and assumed to be pounded by a positive constant. Substituting (50) into (48) yields

$$\tilde{\Gamma} = \tilde{W}^T (A^T \tilde{\omega} + B^T \tilde{b} + C^T \tilde{c} + D^T \tilde{\alpha} + g)$$

$$+ \hat{W}^T (A^T \tilde{\omega} + B^T \tilde{b} + C^T \tilde{c} + D^T \tilde{\alpha} + g) + \tilde{W}^T \hat{\Theta} + \varepsilon$$

$$= \tilde{W}^T A^T (\omega^* - \hat{\omega}) + \tilde{W}^T B^T (b^* - \hat{b}) + \tilde{W}^T C^T (c^* - \hat{c})$$

$$+ \tilde{W}^T D^T (\alpha^* - \hat{\alpha}) + \tilde{W}^T g + \hat{W}^T A^T \tilde{\omega} + \hat{W}^T B^T \tilde{b} \quad (51)$$

$$+ \hat{W}^T C^T \tilde{c} + \hat{W}^T D^T \tilde{\alpha} + \hat{W}^T g + \tilde{W}^T \hat{\Theta} + \varepsilon$$

$$= \tilde{W}^T (\hat{\Theta} - A^T \hat{\omega} - B^T \hat{b} - C^T \hat{c} - D^T \hat{\alpha}) + \tilde{\omega}^T A \hat{W}$$

$$+ \tilde{b}^T A \hat{W} + \tilde{c}^T A \hat{W} + \tilde{\alpha}^T A \hat{W} + \gamma$$

where the uncertain term γ is expressed as $\gamma = \tilde{W}^T A^T \omega^* + \tilde{W}^T B^T b^* + \tilde{W}^T C^T c^* + \tilde{W}^T D^T \alpha^* + \tilde{W}^T g + \varepsilon$.

C. Intelligent Adaptive Backstepping $\mathcal{H}_\infty$ Control System

The proposed intelligent adaptive backstepping $\mathcal{H}_\infty$ control system is shown in Fig. 1, which is comprised an adaptive backstepping controller and a robust $\mathcal{H}_\infty$ controller. The tracking error $e_1(t)$ is defined in (12), a stabilizing function $\alpha_1(t)$ in (14) and $e_2(t)$ in (16). The hybrid control law of the IABHTCS can be rewritten as follows:

$$U_{qs}^*(t) = U_{qs}^{IABC}(t) + U_{qs}^{RC}(t) \quad (52)$$

where $U_{qs}^{IABC}(t)$ is the adaptive backstepping controller and $U_{qs}^{RC}(t)$ is the robust $\mathcal{H}_\infty$ controller.

$$U_{qs}^{IABC}(t) = B_n^{-1}[\ddot{\theta}_r^m(t) - A_n \dot{\theta}_r(t) - \hat{\Gamma}(t)$$
$$- k_1 \dot{e}_1(t) - k_2 e_2(t) - e_1(t)] \quad (53)$$

where $U_{qs}^{DRFWNNC}(t) = \hat{\Gamma}(t)$ is the output of the DRFWNN identifier to estimate the non-linear uncertainties $\Gamma(t)$ online. Substituting of (52) and (53) into (18) yields

$$\dot{e}_2(t) = \Gamma(t) - \hat{\Gamma}(t) - k_2 e_2(t) - e_1 + U_{qs}^{RC}(t) \quad (54)$$

Substituting (51) into (54), we can obtain

$$\dot{e}_2(t) = \tilde{W}^T (\hat{\Theta} - A^T \hat{\omega} - B^T \hat{b} - C^T \hat{c} - D^T \hat{\alpha})$$
$$+ \tilde{\omega}^T A \hat{W} + \tilde{b}^T B \hat{W} + \tilde{c}^T C \hat{W} + \tilde{\alpha}^T D \hat{W} \quad (55)$$
$$+ \gamma - k_2 e_2(t) - e_1 + U_{qs}^{RC}(t)$$

Theorem: Consider the PMSM servo drive represented by (9), if the IABHTCS is designed as (52) where the adaptive backstepping controller is designed as (53), in which the adaptation laws of the DRFWNN uncertainty observer are designed as (56)-(60). As a result, the stability of the proposed control system can be guaranteed.

$$\dot{\hat{W}} = -\dot{\tilde{W}} = \eta_W e_2 (\hat{\Theta} - A^T \hat{\omega} - B^T \hat{b} - C^T \hat{c} - D^T \hat{\alpha}) \quad (56)$$

$$\dot{\hat{\omega}} = -\dot{\tilde{\omega}} = \eta_\omega e_2 A \hat{W} \quad (57)$$

$$\dot{\hat{b}} = -\dot{\tilde{b}} = \eta_b e_2 B \hat{W} \quad (58)$$

$$\dot{\hat{c}} = -\dot{\tilde{c}} = \eta_c e_2 C \hat{W} \quad (59)$$
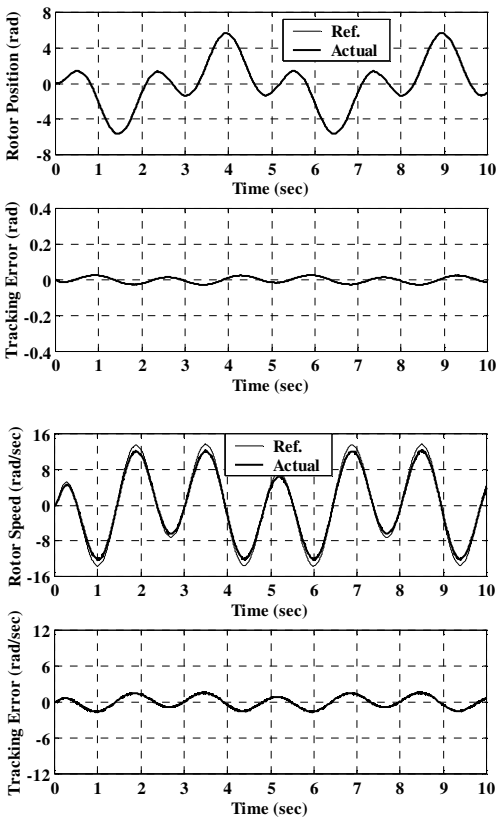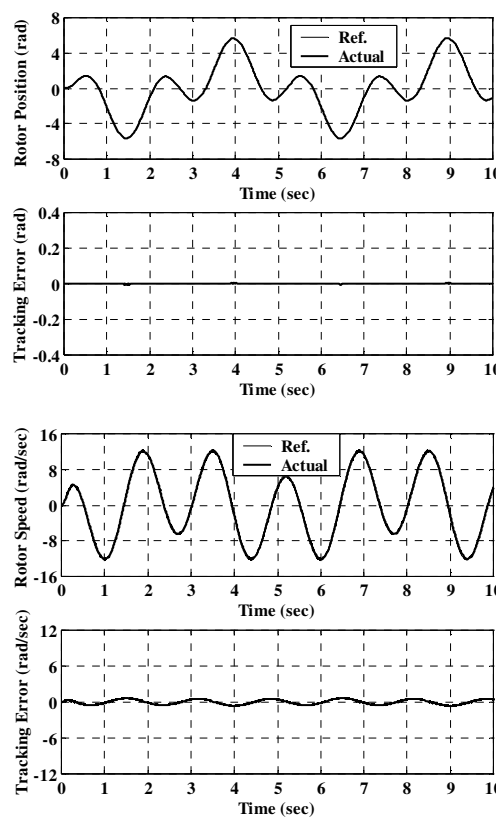
(a) Using backstepping position controller   (b) Using IABHTCS with DRFWNN observer and $\mathcal{H}_\infty$ control

Fig. 4 Dynamic response for the reference position of 2π rad at no-loading for both position controllers at case (1) of parameter uncertainties
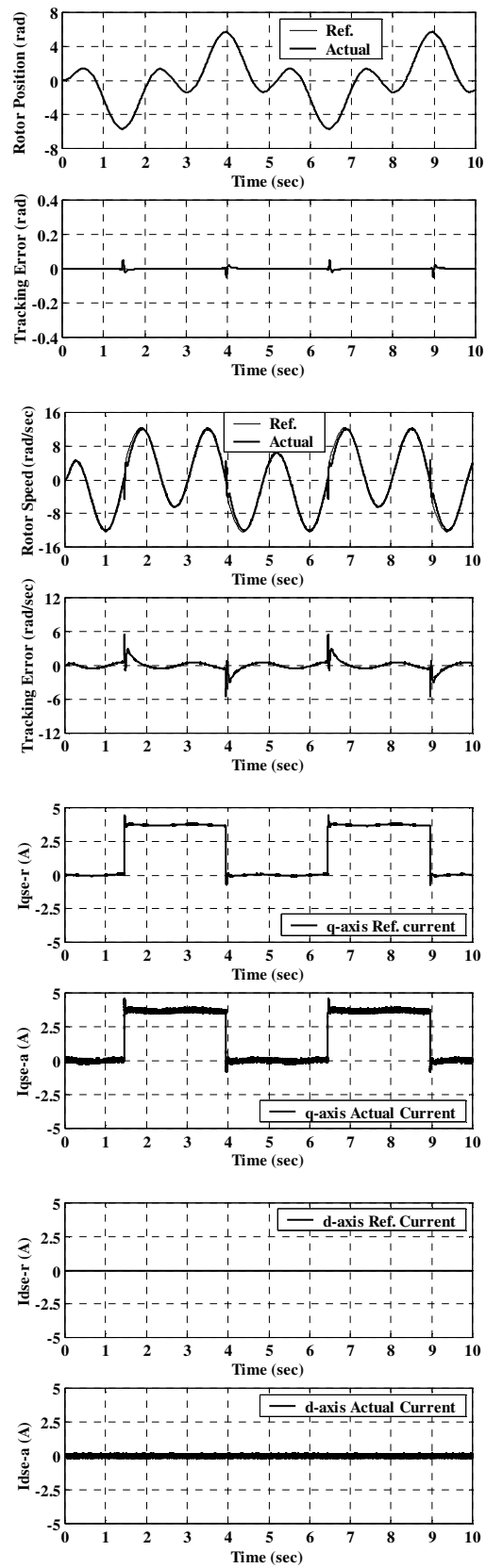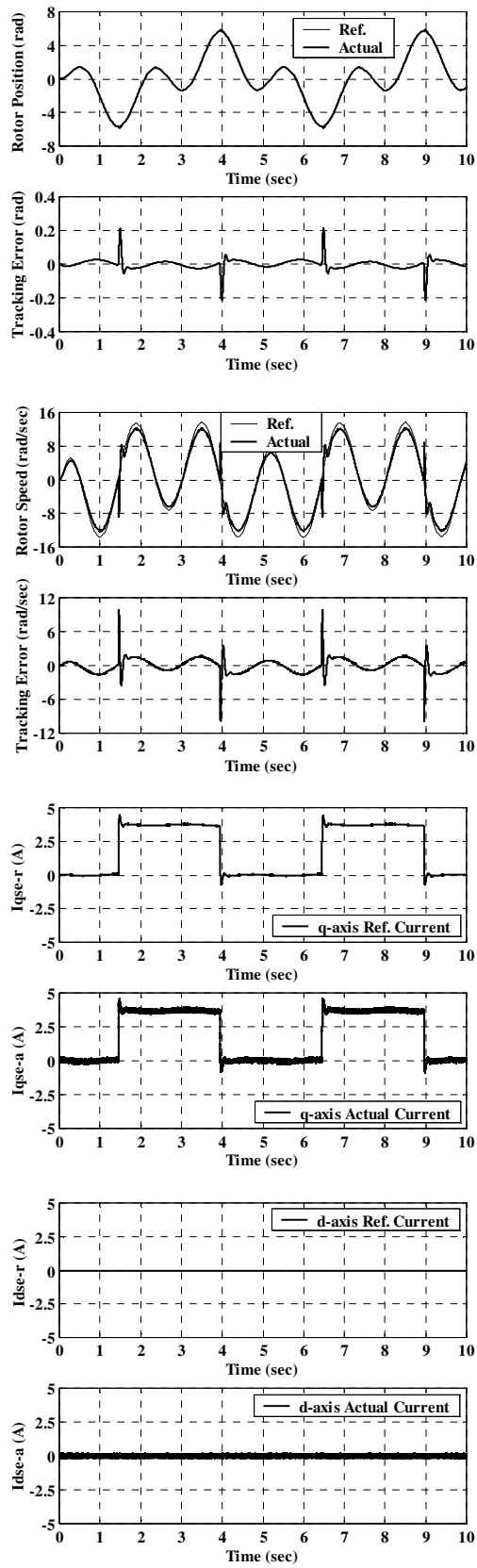
(a) Using backstepping position controller

(b) Using IABHTCS with DRFWNN observer and $\mathcal{H}_\infty$ control

Fig. 5 Dynamic response for the reference position of 2π rad and subsequent loading of 3.6 N.m for both position controllers at case (1) of parameter uncertainties
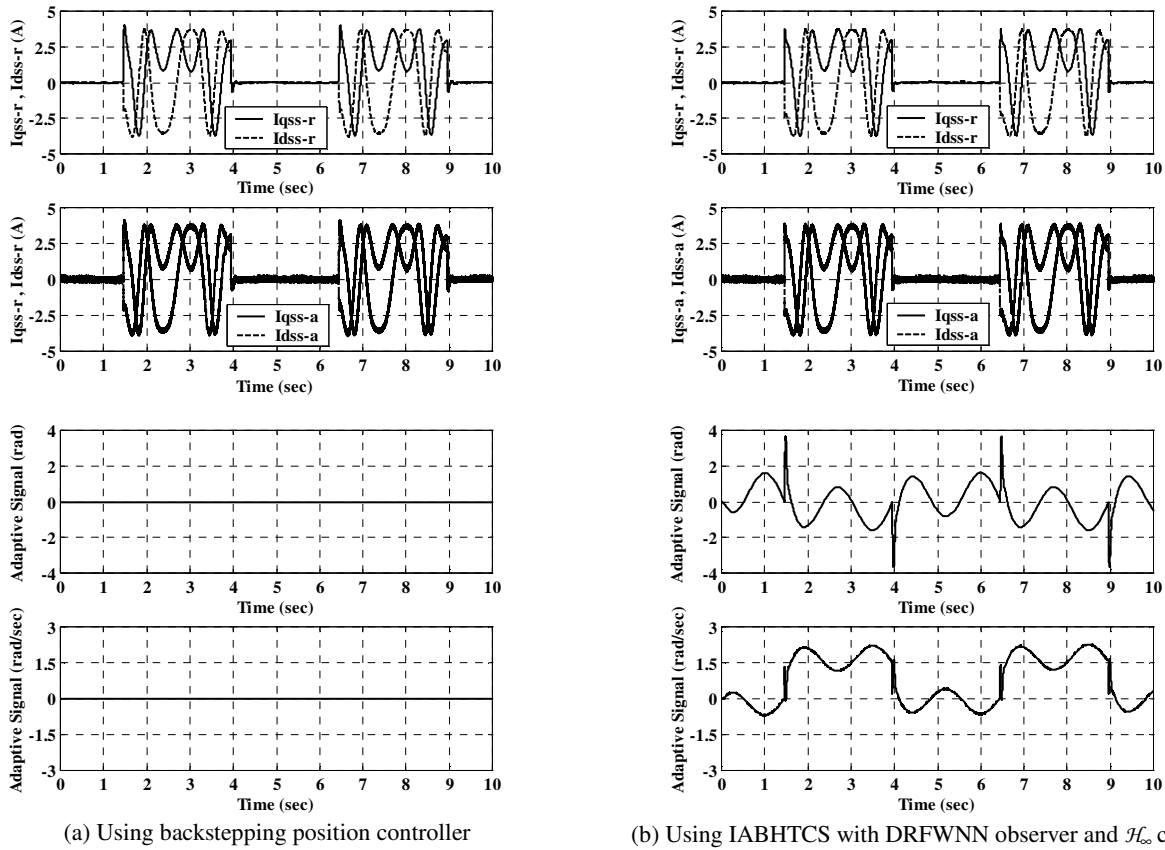
(a) Using backstepping position controller   (b) Using IABHTCS with DRFWNN observer and $\mathcal{H}_\infty$ control

Fig. 5 (*Continued*) Dynamic response for the reference position of 2π rad and subsequent loading of 3.6 N.m for both position controllers at case (1) of parameter uncertainties

$$\dot{\hat{\alpha}} = -\dot{\tilde{\alpha}} = \eta_\alpha e_2 D \hat{W} \tag{60}$$

where η_W, η_ω, η_b, η_c and η_α are strictly positive learning rates and the robust $\mathcal{H}_\infty$ controller is designed as (61).

$$U_{qs}^{RC} = -\frac{1}{2} \cdot \frac{(\delta^2 + 1)}{\delta^2} \cdot e_2 \tag{61}$$

where δ is a prescribed attenuation constant. Then, the PMSM servo drive system guarantees the following properties:

$$k_1 \int_0^T e_1^2(\tau) d\tau = \frac{1}{2} e_1^2(0) \frac{1}{2} e_2^2(0) + \frac{1}{2\eta_W} \tilde{W}^T(0) \tilde{W}(0)$$
$$+ \frac{1}{2\eta_\omega} \tilde{\omega}^T(0) \tilde{\omega}(0) + \frac{1}{2\eta_b} \tilde{b}^T(0) \tilde{b}(0)$$
$$+ \frac{1}{2\eta_c} \tilde{c}^T(0) \tilde{c}(0) + \frac{1}{2\eta_\varepsilon} \tilde{\alpha}^T(0) \tilde{\alpha}(0) + \frac{\delta^2}{2} \int_0^T \gamma^2(\tau) d\tau \tag{62}$$

where $T \in [0, \infty]$. If γ is squared integrable, that is $\int_0^\infty \gamma^2(\tau) d\tau < \infty$, then $\lim_{t \to \infty} |e_1| = 0$.

Proof: Define a Lyapunov function as

$$V_3(t) = V_2(t) + \frac{1}{2\eta_W} \tilde{W}^T \tilde{W} + \frac{1}{2\eta_\omega} \tilde{\omega}^T \tilde{\omega}$$
$$+ \frac{1}{2\eta_b} \tilde{b}^T \tilde{b} + \frac{1}{2\eta_c} \tilde{c}^T \tilde{c} + \frac{1}{2\eta_\varepsilon} \tilde{\alpha}^T \tilde{\alpha} \tag{62}$$

Substitute (15) and (19) into (62) yields

$$V_3(t) = \frac{1}{2} e_1^2(t) + \frac{1}{2} e_2^2(t) + \frac{1}{2\eta_W} \tilde{W}^T \tilde{W} + \frac{1}{2\eta_\omega} \tilde{\omega}^T \tilde{\omega}$$
$$+ \frac{1}{2\eta_b} \tilde{b}^T \tilde{b} + \frac{1}{2\eta_c} \tilde{c}^T \tilde{c} + \frac{1}{2\eta_\varepsilon} \tilde{\alpha}^T \tilde{\alpha} \tag{63}$$

The derivative of $V_3(t)$ and using (13), (16) and (55)-(61) yields

$$\dot{V}_3(t) = e_1(t)\dot{e}_1(t) + e_2(t)\dot{e}_2(t) + \frac{1}{\eta_W} \tilde{W}^T \dot{\tilde{W}} + \frac{1}{\eta_\omega} \tilde{\omega}^T \dot{\tilde{\omega}}$$
$$+ \frac{1}{\eta_b} \tilde{b}^T \dot{\tilde{b}} + \frac{1}{\eta_c} \tilde{c}^T \dot{\tilde{c}} + \frac{1}{\eta_\varepsilon} \tilde{\alpha}^T \dot{\tilde{\alpha}}$$
$$= e_1(t)[-k_1 e_1(t) + e_2(t)] + e_2(t)\{\tilde{W}^T(\hat{\Theta} - A^T\hat{\omega} - B^T\hat{b}$$
$$- C^T\hat{c} - D^T\hat{\alpha}) + \tilde{\omega}^T A\hat{W} + \tilde{b}^T B\hat{W} + \tilde{c}^T C\hat{W} + \tilde{\alpha}^T D\hat{W}$$
$$+ \gamma - k_2 e_2(t) - e_1 + U_{qs}^{RC}(t)\} + \frac{1}{\eta_W} \tilde{W}^T \dot{\tilde{W}} + \frac{1}{\eta_\omega} \tilde{\omega}^T \dot{\tilde{\omega}}$$
$$+ \frac{1}{\eta_b} \tilde{b}^T \dot{\tilde{b}} + \frac{1}{\eta_c} \tilde{c}^T \dot{\tilde{c}} + \frac{1}{\eta_\varepsilon} \tilde{\alpha}^T \dot{\tilde{\alpha}}$$
$$= -k_1 e_1^2(t) - k_2 e_2^2(t) + \tilde{W}^T\{e_2(t)(\hat{\Theta} - A^T\hat{\omega} - B^T\hat{b} - C^T\hat{c}$$
$$- D^T\hat{\alpha}) + \frac{1}{\eta_W} \dot{\tilde{W}}\} + \tilde{\omega}^T\{e_2(t)A\hat{W} + \frac{1}{\eta_\omega} \dot{\tilde{\omega}}\}$$
$$+ \tilde{b}^T\{e_2(t)B\hat{W} + \frac{1}{\eta_b} \dot{\tilde{b}}\} + \tilde{c}^T\{e_2(t)C\hat{W} + \frac{1}{\eta_c} \dot{\tilde{c}}\}$$

$$+\tilde{\alpha}^T\{e_2(t)D\hat{W}+\frac{1}{\eta_\varepsilon}\dot{\tilde{\alpha}}\}+e_2(t)\{\gamma+U_{qs}^{RC}(t)\}$$

$$=-k_1e_1^2(t)-k_2e_2^2(t)+\gamma e_2(t)-\frac{1}{2}\frac{(\delta^2+1)}{\delta^2}\cdot e_2^2(t)$$

$$=-k_1e_1^2(t)-k_2e_2^2(t)-\frac{e_2^2(t)}{2}-\frac{1}{2}\left(\frac{e_2(t)}{\delta}-\gamma\delta\right)^2+\frac{\gamma^2\delta^2}{2}$$

$$\leq-k_1e_1^2(t)+\frac{1}{2}\gamma^2\delta^2$$

(64)

Integrating (64) from $t=0$ to $t=T$, yields

$$V_3(T)-V_3(0)\leq-k_1\int_0^T e_1^2(\tau)d\tau+\frac{\delta^2}{2}\int_0^T\gamma^2(\tau)d\tau \qquad (65)$$

Since $V_3(T)\geq 0$, (65) implies the following:

$$k_1\int_0^T e_1^2(\tau)d\tau\leq V_3(0)+\frac{\delta^2}{2}\int_0^T\gamma^2(\tau)d\tau \qquad (66)$$

Using (63), the above inequality (66) is equivalent to (62). Since $V_3(0)$ is finite, if the approximation error $\gamma\in L_2$, that is $\int_0^T\gamma^2(\tau)d\tau<\infty$, using the Barbalat's lemma [76], [77], it implies that $\lim_{t\to\infty}|e_1|=0$. If the system starts with initial conditions $e_1(0)=0$, $\tilde{W}(0)=0$, $\tilde{\omega}(0)=0$, $\tilde{b}(0)=0$, $\tilde{c}(0)=0$ and $\tilde{\alpha}(0)=0$, then the $\mathcal{H}_\infty$ tracking performance in (62) can be written as

$$\sup_{\gamma\in L_2[0,T]}\frac{\|e_1\|^2}{\|\gamma\|^2}\leq\frac{\delta^2}{2k_1} \qquad (67)$$

where $\|e_1\|^2=\int_0^T e_1^2(\tau)d\tau$, $\|\gamma\|^2=\int_0^T\gamma^2(\tau)d\tau$ and the L_2-gain from γ to the tracking error $e_1(t)$ must equal to or less than a level $\delta^2/2k_1$ [16], [53], [57], [58]. The attenuation constant δ can be specified to achieve the desired attenuation ratio between $\|e_1\|$ and $\|\gamma\|$. Then, the desired robust tracking performance in (62) can be achieved for a prescribed attenuation level δ.
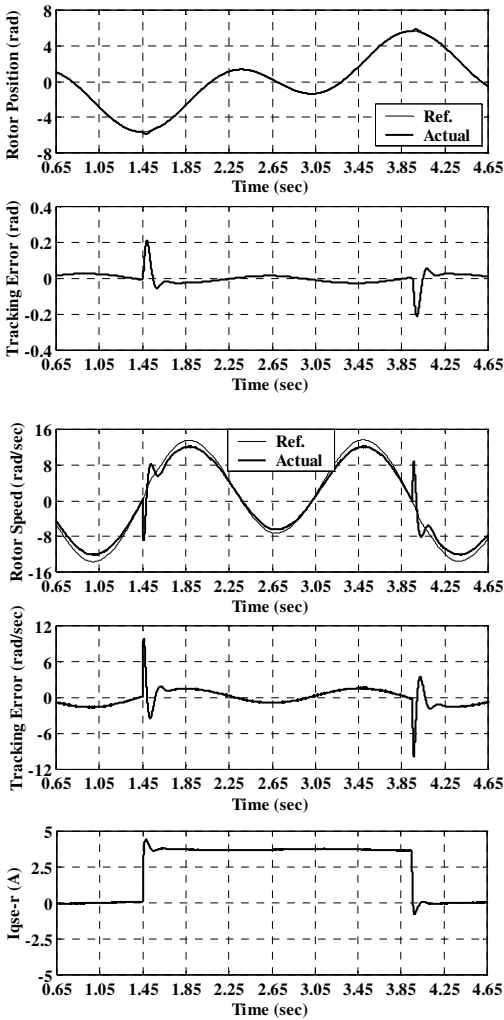
(a) Using backstepping position controller
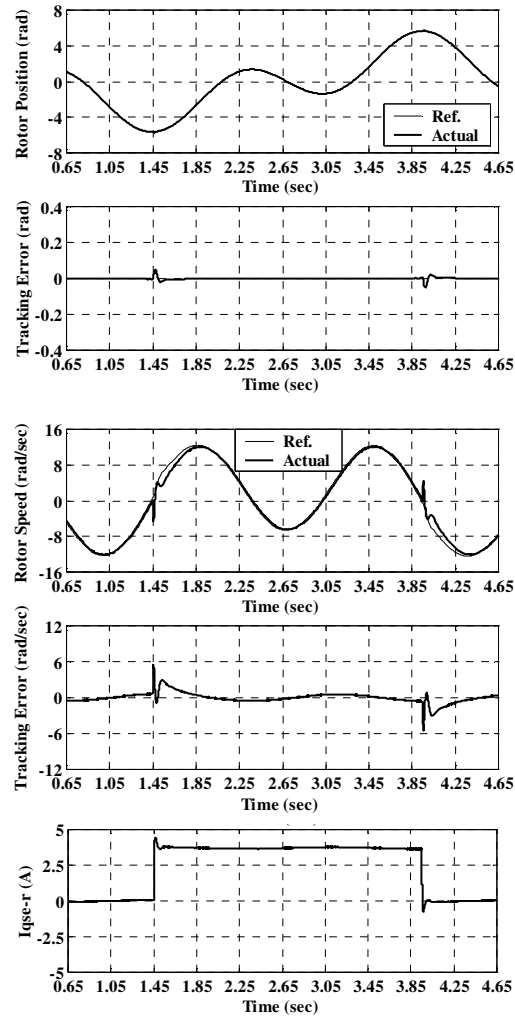
(b) Using IABHTCS with DRFWNN observer and $\mathcal{H}_\infty$ control

Fig. 6 Enlarge dynamic response for the reference position of 2π rad and subsequent loading of 3.6 N.m for both position controllers at case (1) of parameter uncertainties

(a) Using backstepping position controller   (b) Using IABHTCS with DRFWNN observer and $\mathcal{H}_\infty$ control
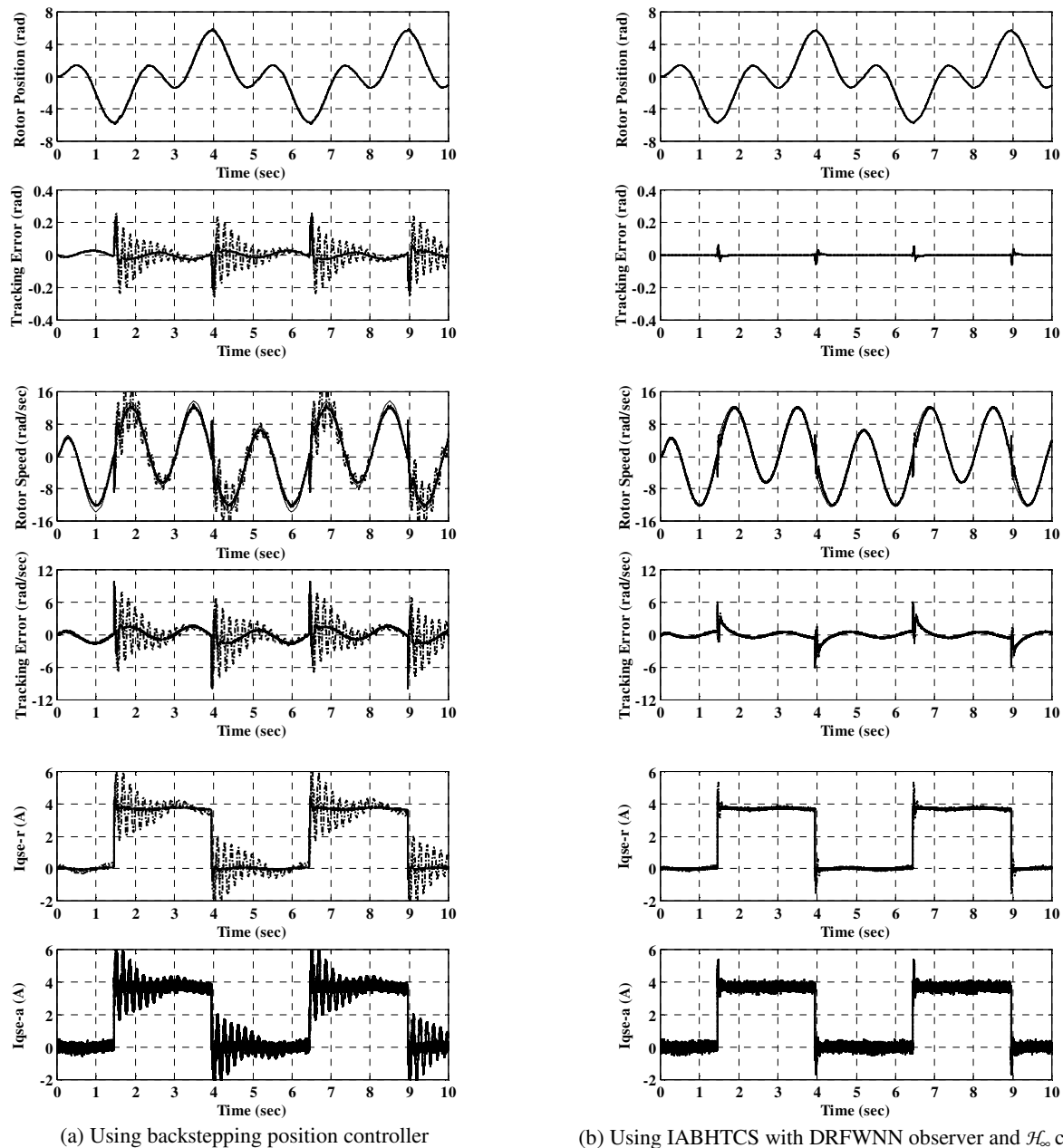
Fig. 7 Dynamic response for the reference position of 2π rad and subsequent loading of 3.6 N.m for both position controllers at different cases (1~4) of PU

IV. NUMERICAL SIMULATION AND EXPERIMENTAL RESULTS

In order to investigate the effectiveness of the proposed tracking control scheme, the simulation and experimentation of the proposed IABHTCS and the backstepping controller are carried out using MATLAB/SIMULINK package based on the control system shown in Figs. 1 and 3. A DSP control board dSPACE DS1102, which is based on a TMS320C31 and TMS320P14 DSPs, is installed in the control computer which includes multi-channels of ADC, DAC, PIO and encoder interface circuits. Digital filter and frequency multiplied by four circuits are built into the encoder interface circuits to increase the precision of the speed and the position feedback

signals and coordinate transformations. The sampling rate is chosen as $200\mu s$ and hence, the carrier frequency of the PWM inverter is 5 kHz. The control interval of the position control loop is set at 1ms. The current-regulated PWM VSI is implemented using Mitsubishi intelligent power module (IPM) using IGBTs with rating of 50A, 1200V and a switching frequency of 15 kHz and driven by a six SEMIKRON IGBT drivers. The speed acquisition has been performed with a 10000 pulses/revolution incremental optical encoder. Therefore, the output of the frequency multiplier circuit is 40000 pulses/revolution which results high precision of the speed/position measurement.

(a) Using backstepping position controller

(b) Using IABHTCS with DRFWNN uncertainty observer and $\mathcal{H}_\infty$ control
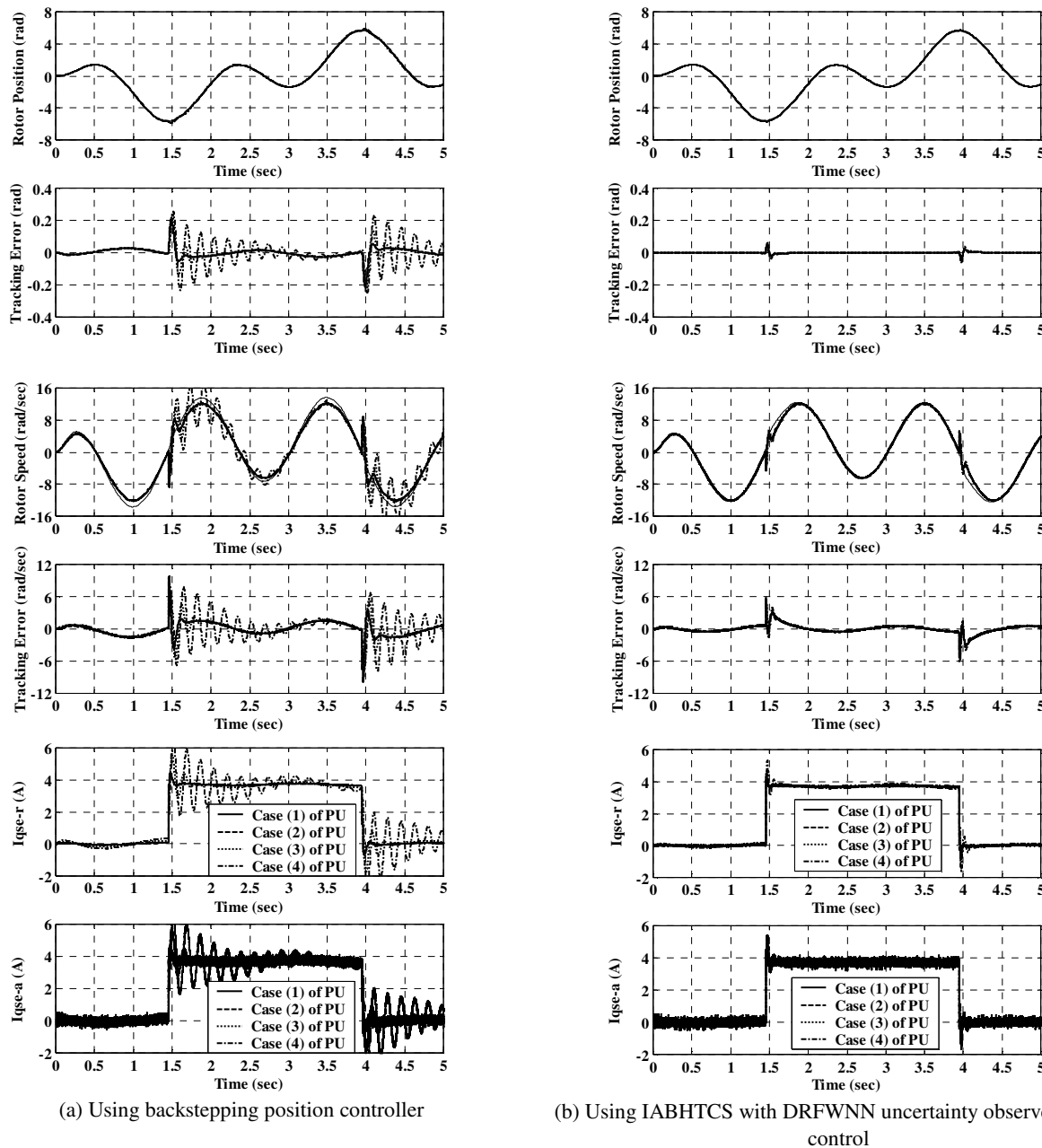
Fig. 8 Enlarge dynamic response for the reference position of 2π rad and subsequent loading of 3.6 N.m for both position controllers at cases (1~4) of PU

A. Numerical Simulation of the PMSM Servo Drive System

The simulations results of the PMSM drive system are presented to verify the feasibility of the proposed IABHTCS under various operating conditions. To investigate the robustness of the proposed controllers, four cases including PU and external load disturbance are considered.

Case 1: $1.0\times(L_s/R_s)$, $1.0\times(\beta_m/J_m)$, $1.00\times\lambda_m$, T_L=0–3.6 N.m

Case 2: $0.5\times(L_s/R_s)$, $1.5\times(\beta_m/J_m)$, $0.85\times\lambda_m$, T_L=0–3.6 N.m

Case 3: $1.5\times(L_s/R_s)$, $2.5\times(\beta_m/J_m)$, $1.25\times\lambda_m$, T_L=0–3.6 N.m

Case 4: $1.5\times(L_s/R_s)$, $5.0\times(\beta_m/J_m)$, $1.25\times\lambda_m$, T_L=0–3.6 N.m

The dynamic performance of the PMSM servo drive due to reference model command of 2π rad under no-loading for the backstepping controller alone at case (1) of PU including the responses of the reference model and rotor position, the tracking position error, rotor speed, the tracking speed error, are predicted as shown in Fig. 4 (a), respectively. On the other hand, the dynamic performance of the PMSM servo drive using the IABHTCS is shown in Fig. 4(b) at case (1) of PU. The results obtained in Fig. 4 illustrate good dynamic performances, in command tracking, are realized for both position tracking controllers. Improvement of the control performance by addition the proposed IABHTCS can be observed from the obtained results. From these results, it clear that the tracking position and speed errors with the backstepping controller is larger than the obtained ones using the proposed intelligent adaptive $\mathcal{H}_\infty$ controller.

(a) Using backstepping position controller

(b) Using IABHTCS with DRFWNN uncertainty observer and $\mathcal{H}_\infty$ control
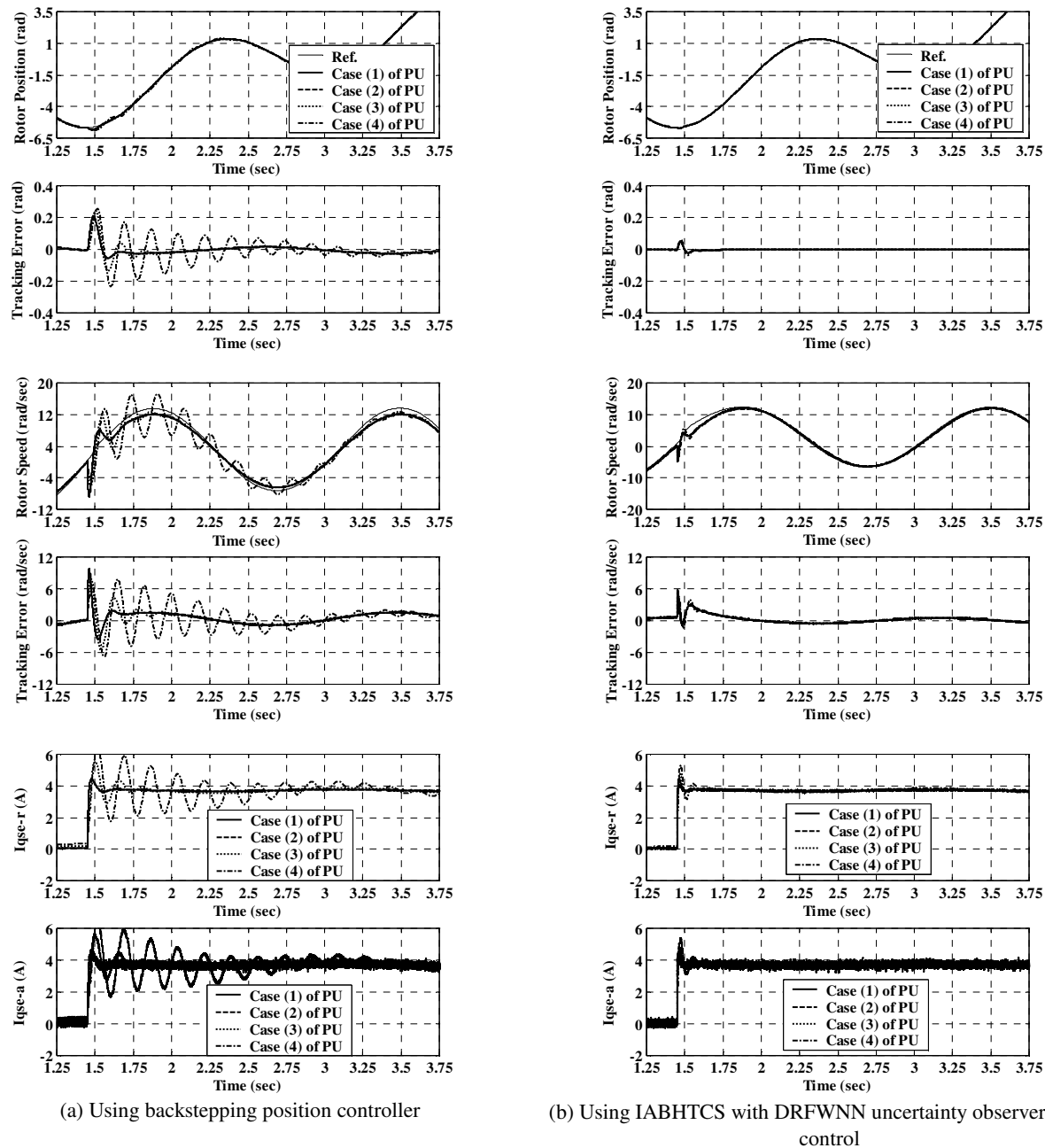
Fig. 9 Enlarge dynamic response for the reference position of 2π rad and subsequent loading of 3.6 N.m for both position controllers at cases (1~4) of PU

To testify the robustness against external load disturbance, the dynamic performance of the PMSM servo drive due to reference model command of 2π rad under subsequent loading of 3.6 N.m for the backstepping controller alone at case (1) of PU including the responses of the reference model and rotor position, the tracking position error, rotor speed, the tracking speed error, d-q axis current response and adaptive signals are predicted as shown in Fig. 5(a), respectively. On the other hand, the dynamic performance of the PMSM servo drive using the IABHTCS is shown in Fig. 5(b) at case (1) of PU. The disturbance rejection capabilities have been checked when a load of 3.6 N.m is applied to the shaft at t = 1.45 sec.

Enlarge dynamic response of the PMSM servo drive for both position controllers at the same operating condition is shown in Fig. 6. The results obtained in Figs. (5) and (6) illustrate good dynamic performances, in command tracking and load regulation performance, are realized for both position tracking controllers. Improvement of the control performance by addition the proposed IABHTCS can be observed from the obtained results in command tracking and load regulation characteristics. From these results, it clear that the tracking position and speed errors with the backstepping controller is larger than the obtained ones using the proposed intelligent adaptive $\mathcal{H}_\infty$ controller.

(a) Using backstepping position controller   (b) Using IABHTCS with DRFWNN observer and $\mathcal{H}_\infty$ control
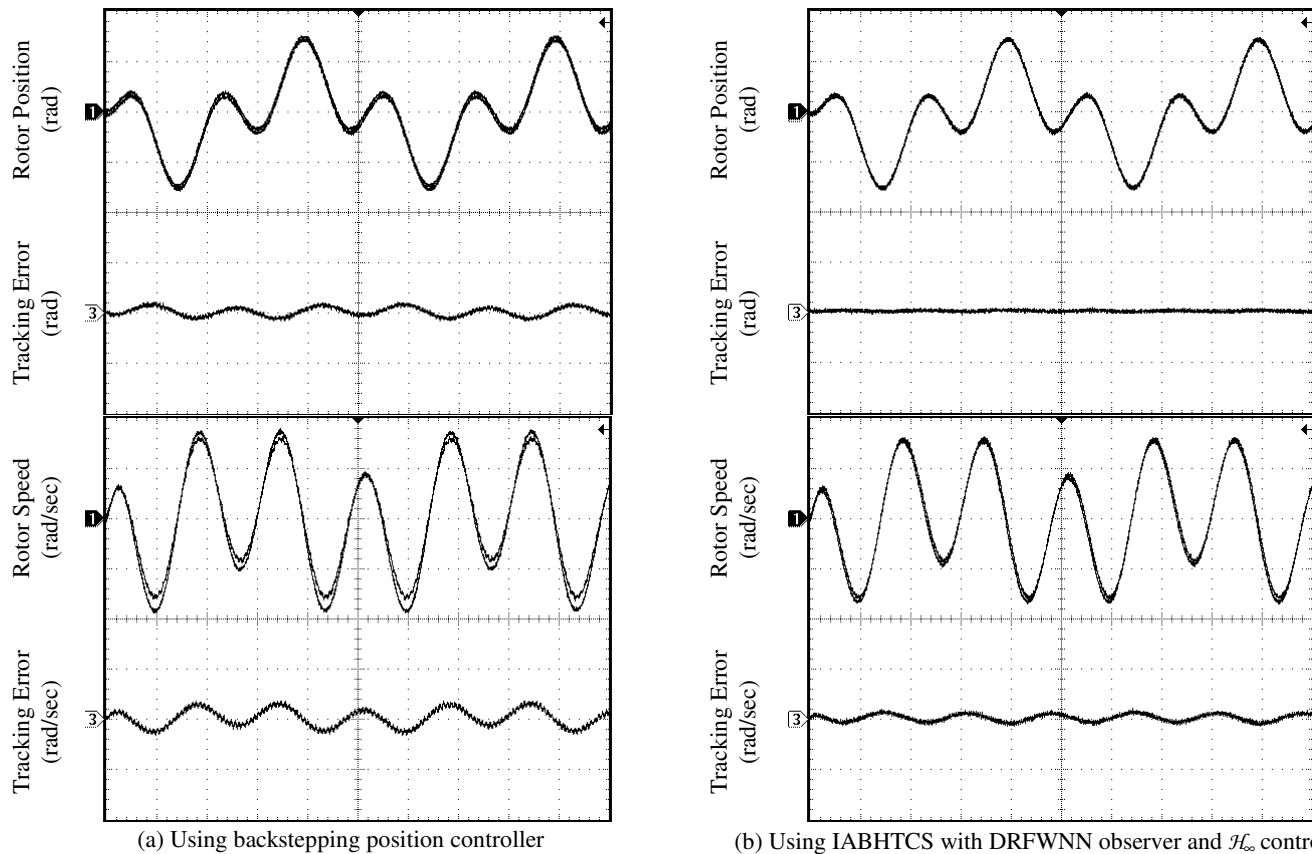
Fig. 10 Experimental results of the dynamic response for a reference position of 2π rad at no-loading for both position controllers: position response 4 rad/div, speed response 8 (rad/sec)/div, tracking position error 0.2 rad/div, tracking speed error 6 (rad/sec)/div, time base for all traces 1 sec/div at case (1) of PU

To further verify the performance robustness of the proposed control schemes, four cases of PU and external load disturbance are considered, Cases (1~4), for comparison. The dynamic performance of the PMSM servo drive for both backstepping controller and the IABHTCS using dynamic recurrent fuzzy-wavelet-neural-network at all cases of PU is predicted in Fig. 7. Enlarge dynamic response of the PMSM servo drive for both position controllers at the same operating conditions are shown in Figs. (8) and (9). Furthermore, the maximum tracking position errors at nominal parameters, case (1) of PU is approximately 0.2103 rad, for the proposed backstepping control system. On the other hand, the one with the IABHTCS at the same case is approximately constants and equal 0.05232 rad. The maximum position regulation dips at four cases of PU are 0.2103 rad, 0.2106 rad, 0.2425 rad, and 0.2551 rad, respectively for the backstepping controller. On the other hand, the ones with the IABHTCS at four cases (1~4) of PU are 0.05232 rad, 0.04842 rad, 0.05542 rad and 0.05965 rad, respectively. From the simulation results shown in Fig. 7, the tracking errors converge quickly and the robust control characteristics of the proposed IABHTCS under the occurrence of PU can be clearly observed. Compared with the backstepping controller, the tracking errors and regulation characteristics are much reduced. Therefore, the proposed controller with intelligent uncertainty observer can yield superior control performance than the backstepping control

scheme. As a result, the proposed IABHTCS provides a rapid and accurate response for the reference model under load changes within 0.30 sec compared with the backstepping controller which has sluggish recovery time of more than 2.50 sec at case (4) of PU. Thus, it can be verified that the proposed intelligent adaptive backstepping controller at all cases of PU can satisfy the robustness, the accuracy requirements and is more suitable in the tracking control of the PMSM servo drive system.

B. Experimentation of the PMSM Servo Drive System

To further verify the performance of the proposed control schemes applied to the PMSM servo drive in practical applications, some experimental results are introduced. The experimental results of the dynamic performance for the backstepping controller due to reference model command under no-loading at case (1) of PU including the responses of the reference model and rotor position, the tracking position error, rotor speed, the tracking speed error are predicted in Fig. 10(a), respectively. On the other hand, the experimental results of the PMSM servo drive using the proposed IABHTCS is shown in Fig. 10(b) at the same conditions. The experimental results obtained in Fig. 10 clearly illustrate good dynamic performances, in command tracking, are realized for both position tracking controllers. Compared with the backstepping controller, the tracking errors are much reduced using the proposed IABHTCS.
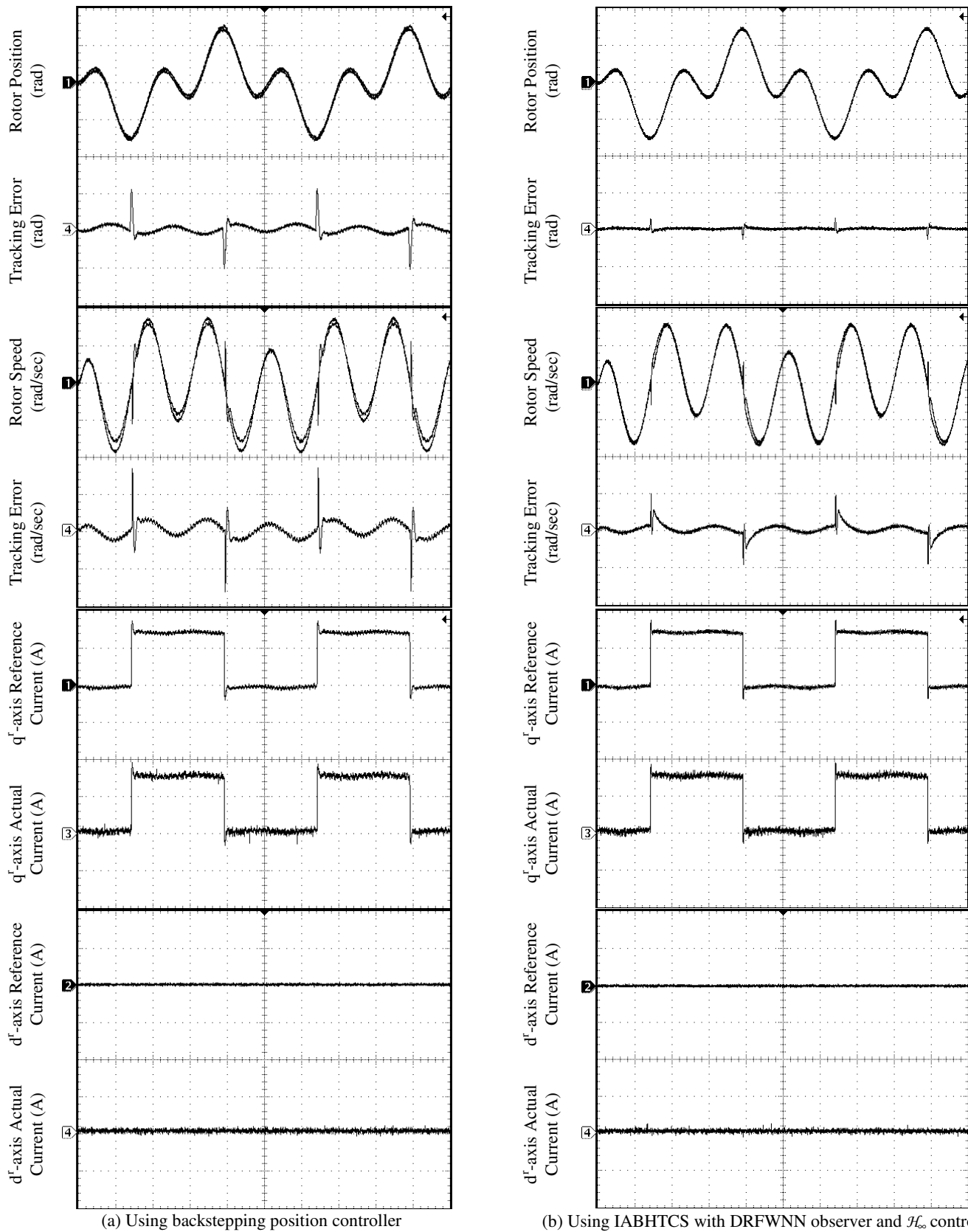
(a) Using backstepping position controller   (b) Using IABHTCS with DRFWNN observer and $\mathcal{H}_\infty$ control

Fig. 11 Experimental results of the dynamic response for a reference position of 2π rad and subsequent loading of 3.6 N.m for both position controllers: position response 4 rad/div, speed response 8 (rad/sec)/div, tracking position error 0.2 rad/div, tracking speed error 6 (rad/sec)/div, adaptive position signal 2 rad/div, adaptive speed signal 1.5 (rad/sec)/div, q-d axis current response 2.5 A/div, time base for all traces 1 sec/div at case (1) of PU

(a) Using backstepping position controller

(b) Using IABHTCS with DRFWNN observer and $\mathcal{H}_\infty$ control
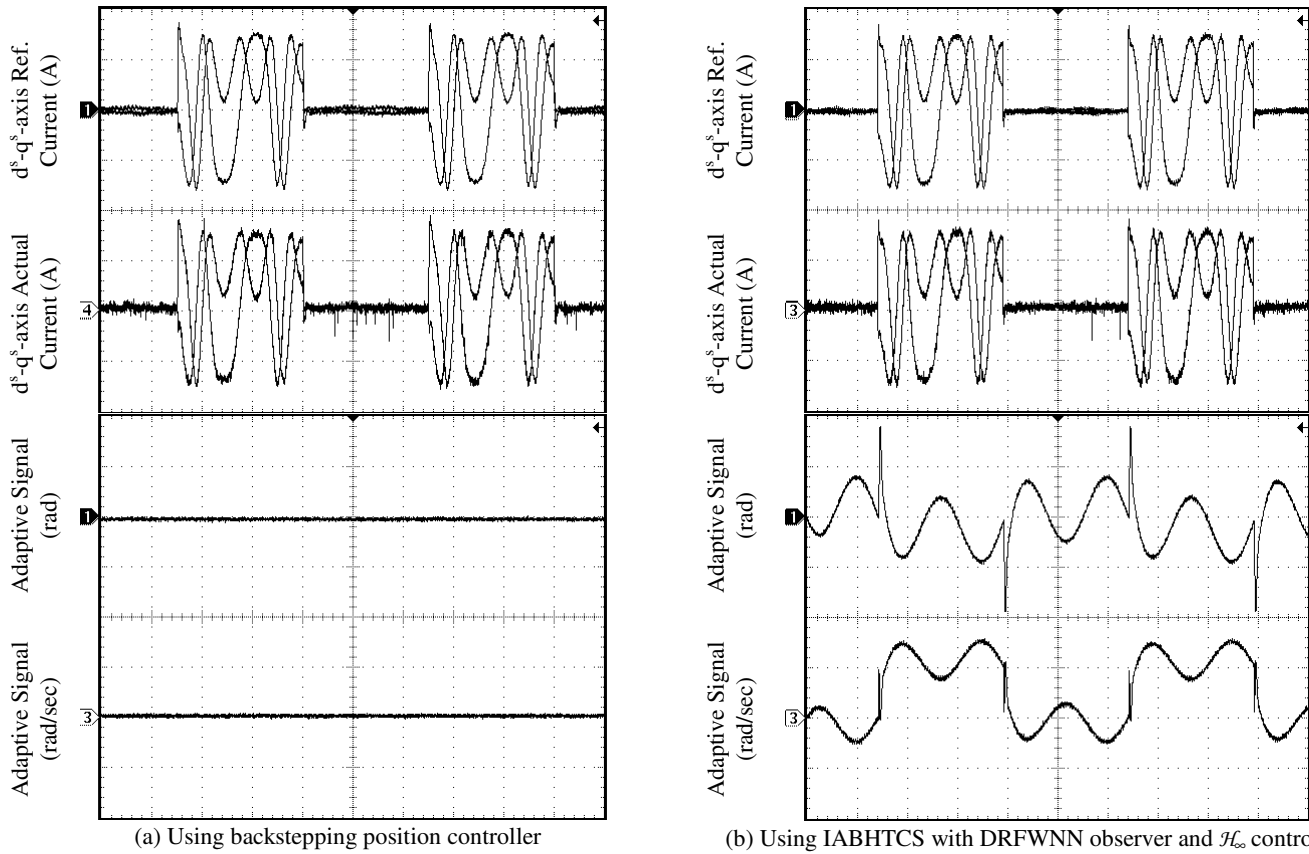
Fig. 11 (*Continued*) Experimental results of the dynamic response for a reference position of 2π rad and subsequent loading of 3.6 N.m for both position controllers: position response 4 rad/div, speed response 8 (rad/sec)/div, tracking position error 0.2 rad/div, tracking speed error 6 (rad/sec)/div, adaptive position signal 2 rad/div, adaptive speed signal 1.5 (rad/sec)/div, q-d axis current response 2.5 A/div, time base for all traces 1 sec/div at case (1) of PU

To testify the external load disturbance, the experimental results of the dynamic performance for the backstepping controller due to reference model command under subsequent loading of 3.6 N.m at case (1) of PU including the responses of the reference model and rotor position, the tracking position error, rotor speed, the tracking speed error, d-q axis current response and adaptive signals are predicted in Fig. 11(a), respectively. On the other hand, the experimental results of the PMSM servo drive using the proposed IABHTCS is illustrated in Fig. 11(b) at the same conditions. Furthermore, the disturbance rejection capabilities have been checked for both position controllers. Enlarge dynamic response of the PMSM servo drive for both position controllers at the same operating condition is shown in Fig. 12. In addition, the maximum tracking position errors at case (1) of PU is approximately 0.2104 rad, for the backstepping controller. On the other hand, the one with the IABHTCS at case (1) of PU is approximately 0.05235 rad. The experimental results obtained in Figs. (11) and (12) clearly illustrate good dynamic performance, in command tracking and load regulation performance, are realized for both position tracking controllers. Compared with the backstepping controller, the tracking errors and regulation characteristics are much reduced for the proposed IABHTCS. Therefore, it can yield superior control performance than the

backstepping controller. As a result, the proposed IABHTCS provides a rapid and accurate response for the reference model under load changes within 0.3 sec compared with the backstepping position tracking controller which has sluggish recovery time of more than 1.50 sec at case (1) of PU. It is obvious that the performance of the PMSM servo drive system is improved greatly by using the IABHTCS. Thus, it can be verified that the proposed intelligent adaptive $\mathcal{H}_\infty$ controller can satisfy the accuracy requirements and is more suitable in the tracking control of the PMSM servo drive system for practical applications.

C. Performance Measure of the PMSM Servo Drive

To measure the performance of the servo drive, the maximum tracking error, TE_{max}, the average tracking error, TE_{mean} and the standard deviation of the tracking error, T_{sd}, are defined as follows:

$$TE_{\max} = \max_{k} \sqrt{T(k)^2} \tag{68}$$

$$TE_{mean} = \sum_{k=1}^{n} \frac{T(k)}{n} \tag{69}$$

$$TE_{sd} = \sqrt{\sum_{k=1}^{n} \frac{(T(k) - T_{mean})^2}{n}} \tag{70}$$

(a) Using backstepping position controller   (b) Using IABHTCS with DRFWNN observer and $\mathcal{H}_\infty$ control
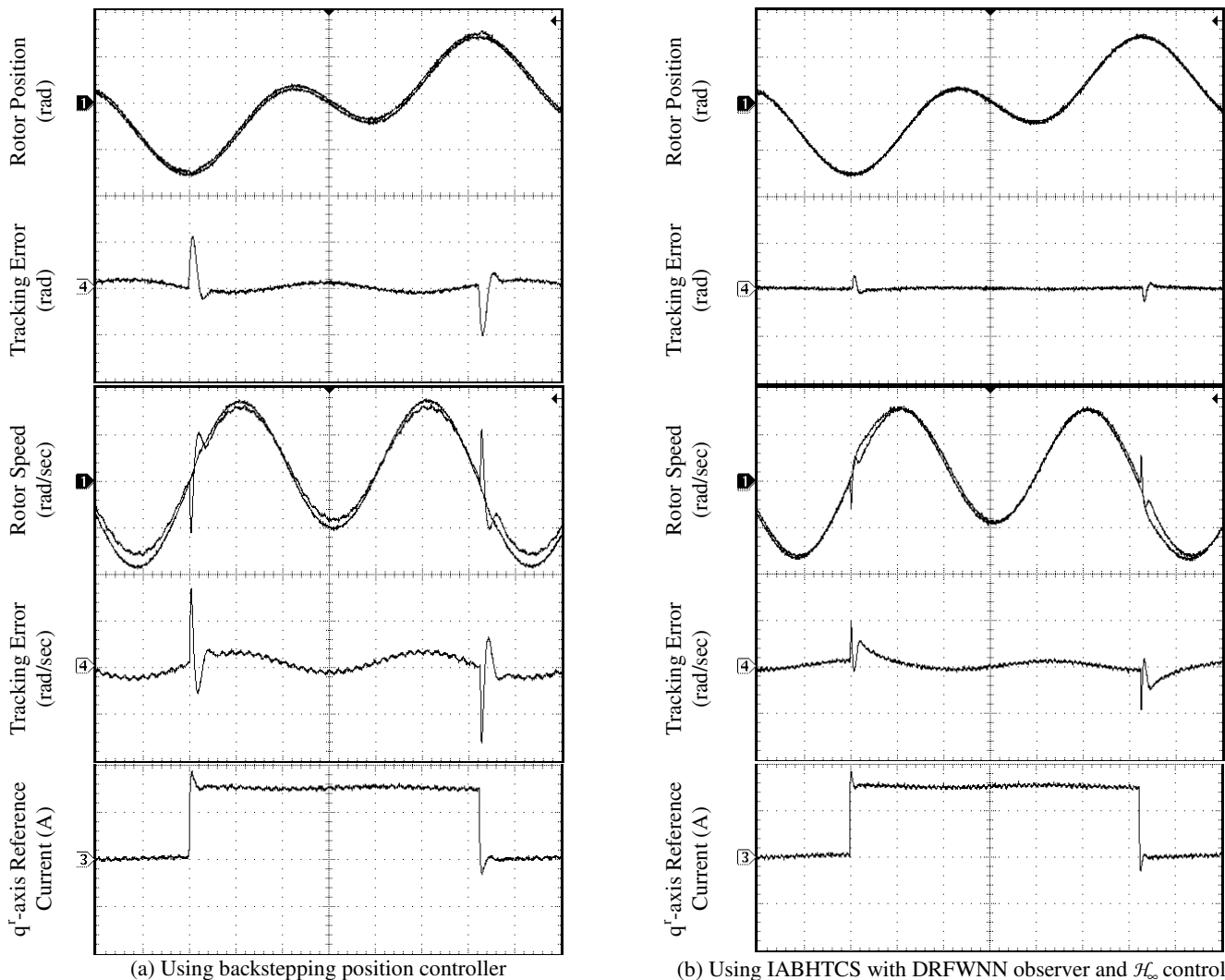
Fig. 12 Enlarge experimental results of the dynamic response for a reference position of 2π rad and subsequent loading of 3.6 N.m for both position controllers: position response 4 rad/div, speed response 8 (rad/sec)/div, tracking position error 0.2 rad/div, tracking speed error 6 (rad/sec)/div, adaptive position signal 2 rad/div, adaptive speed signal 1.5 (rad/sec)/div, q-d axis current response 2.5 A/div, time base for all traces 1 sec/div at Case (1) of PU

where $T(k) = [\theta_r^m(k) - \theta_r(k)]$. The comparison of the control performance can be easily demonstrated using (68)-(70). The performance measures can be easily demonstrated using the TE_{max} and the TE_{mean}. Moreover, the oscillation of the position tracking error can be measured using TE_{sd}. To further investigate the improvement of the proposed IABHTCS, the performance measures of the backstepping controller and IABHTCS are compared and summarized in Tables II, III and IV for simulation and Tables V, VI and VII for experimentation. Tables II and III include the maximum tracking errors, average tracking errors and the standard deviation of the tracking errors at the four cases of parameters uncertainties in simulation whereas Table IV illustrates the percentage reductions in the tracking errors for IABHTCS with respect to IBC control scheme at the same operating conditions. Tables V and VI show the maximum tracking errors, average tracking errors and the standard deviation of the tracking errors at the nominal parameters of the PMSM

servo drive system, case (1) in experimentation. From these results, one can easily observe that high values of TE_{max}, TE_{mean} and TE_{sd} have been successfully reduced by the proposed IABHTCS. As well, Table VII shows the percentage reductions in the tracking errors for IABHTCS with respect to the IBC control scheme at case (1) of parameters uncertainties in experimentation. Therefore, the IABHTCS with adaptive DRFWNN uncertainty observer and $\mathcal{H}_\infty$ control methodology possesses the best robust control characteristics and can control the PMSM servo drive system effectively.

D. Comparison of Control Performance

To further investigate the improvement of the proposed IABHTCS, the performance measures of the IBC and IABHTCS at the four cases of PU in simulation and case (1) of PU in experimentation are compared as illustrated in Figs. (13) and (14). The percentage reductions in the tracking errors for IABHTCS with respect to IBC control scheme are given in Figs. (15) and (16). From these results, one can easily observe

that all values of TE_{max}, TE_{mean} and TE_{sd} have been successfully reduced by the proposed IABHTCS.

TABLE II Performance Measures of the IBC under Parameters Uncertainties of PMSM Servo Drive (Simulation)

Parameters Uncertainties	Tracking Errors (rad)		
	Maximum	Average	S.D.
Case (1)	0.2103	0.0002138	0.03239
Case (2)	0.2106	0.0001767	0.03262
Case (3)	0.2425	0.0001363	0.04077
Case (4)	0.2551	0.0002250	0.07303

TABLE III Performance Measures of the IABHTCS under Parameters Uncertainties of PMSM Servo Drive (Simulation)

Parameters Uncertainties	Tracking Errors (rad)		
	Maximum	Average	S.D.
Case (1)	0.05232	2.306e-005	0.005824
Case (2)	0.04842	2.323e-005	0.005582
Case (3)	0.05542	2.322e-005	0.006120
Case (4)	0.05965	2.348e-005	0.006905
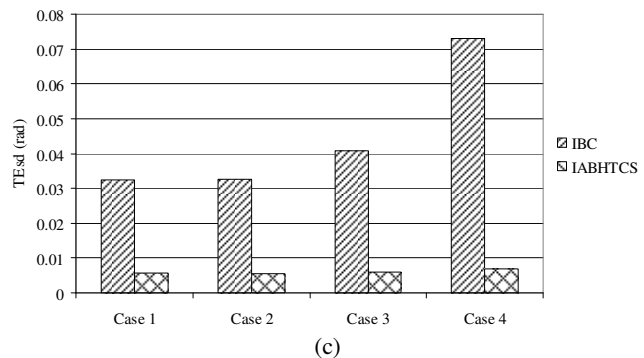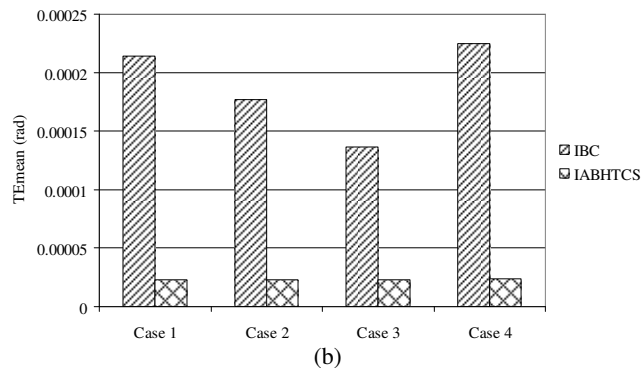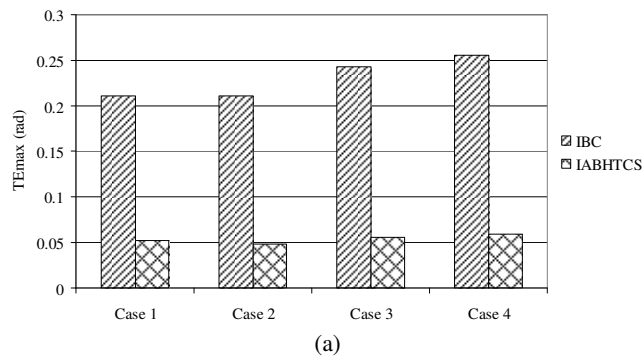
TABLE IV Tracking Errors Reduction of the IABHTCS with respect to the IBC for PMSM Servo Drive (Simulation)

Parameters Uncertainties	Tracking Errors Reduction (%)		
	Maximum	Average	S.D.
Case (1)	75.10	89.21	82.02
Case (2)	77.00	86.85	82.89
Case (3)	77.65	82.96	84.99
Case (4)	76.62	89.56	90.55

TABLE V Performance Measures of the IBC under Nominal Parameters of PMSM Servo Drive (Experimentation)

Nominal Parameters	Tracking Errors (rad)		
	Maximum	Average	S.D.
Case (1)	0.2104	0.0002141	0.03243

TABLE VI Performance Measures of the IABHTCS under Nominal Parameters of PMSM Servo Drive (Experimentation)

Nominal Parameters	Tracking Errors (rad)		
	Maximum	Average	S.D.
Case (1)	0.05235	2.310e-005	0.005830

Fig. 13 Performance measures of IBC and IABHTCS and $\mathcal{H}_\infty$ control for PMSM servo drive (Simulation)
(a) TE_{max} (b) TE_{mean} (c) TE_{sd}
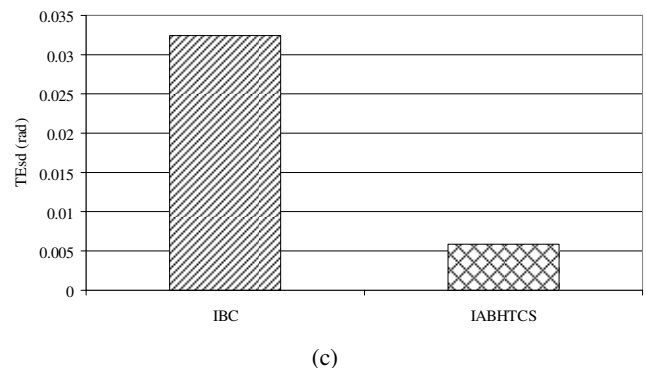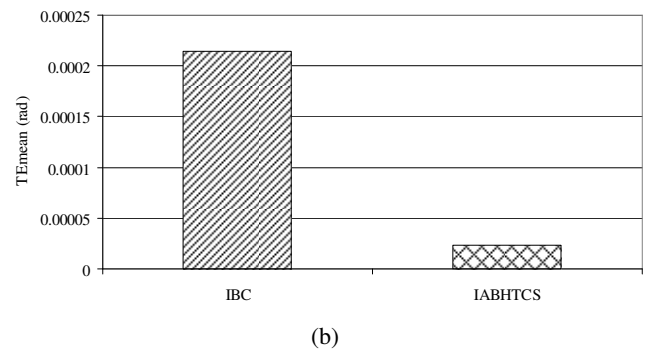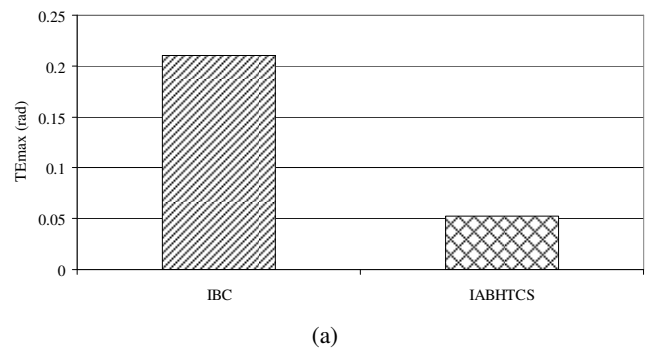
Fig. 14 Performance measures of IBC and IABHTCS and $\mathcal{H}_\infty$ control for PMSM servo drive (Experimentation)
(a) TE_{max} (b) TE_{mean} (c) TE_{sd}
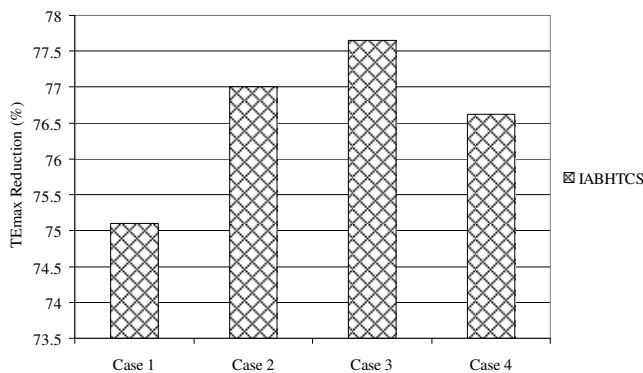
(a)
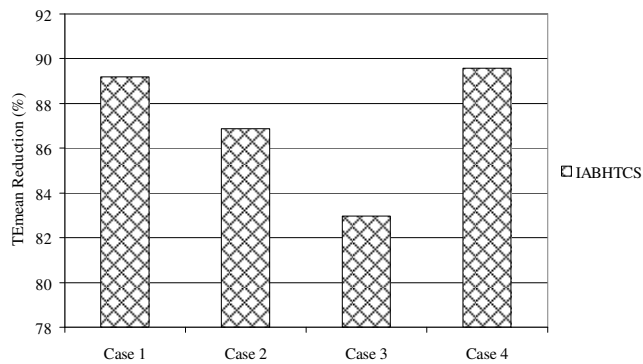
(b)
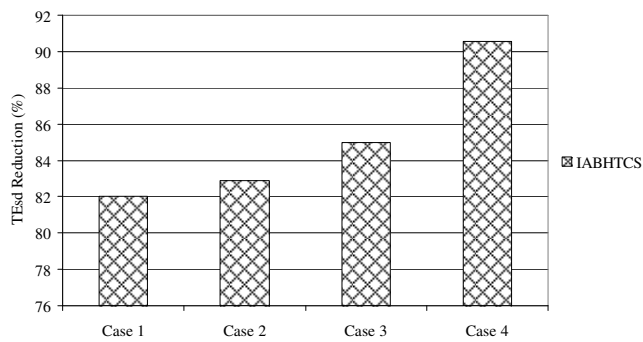
(c)

Fig. 15 Tracking errors reduction using IABHTCS with respect to
IBC for PMSM servo drive (Simulation)
(a) TE_{max} (b) TE_{mean} (c) TE_{sd}
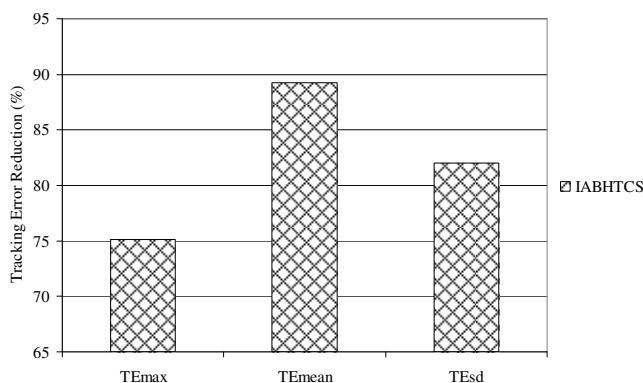
Fig. 16 Tracking errors reduction using IABHTCS with respect to
IBC for PMSM servo drive (Experimentation)

TABLE VII Tracking Errors Reduction of the IABHTCS under
Nominal Parameters (case (1)) with respect to the IBC for PMSM
Servo Drive (Experimentation)

Controller Type	Tracking Errors Reduction (%)		
	Maximum	Average	S.D.
IBC	Itself	Itself	Itself
IABHTCS	75.11	89.21	82.02

V. CONCLUSIONS

This paper proposed a high-precision intelligent adaptive backstepping $\mathcal{H}_\infty$ control system to control the rotor position of the PMSM servo drive, which guarantees the robustness in the presence of parameter uncertainties, and load disturbances. The proposed control scheme comprises a backstepping controller, a DRFWNN uncertainty observer and a robust $\mathcal{H}_\infty$ controller to improve the performance of the of the PMSM servo drive. The backstepping controller with the intelligent uncertainty observer is used as the main tracking controller and the robust $\mathcal{H}_\infty$ controller is designed to recover the residual of the approximation error via the DRFWNN control system approximation such that the stability of the servo drive system can be guaranteed. In addition, the DRFWNN uncertainty observer is used to adaptively estimate the non-linear uncertainties. The online adaptive control laws are derived based on the Lyapunov stability theorem and $\mathcal{H}_\infty$ control theory so that the stability of the PMSM servo drive can be guaranteed. The simulated and experimental results confirm that the proposed IABHTCS grants robust performance and precise dynamic response to the reference model regardless of load disturbances and PMSM parameter uncertainties. Finally, the main contribution of this paper is the successful development, application and implementation of the IABHTCS with adaptive DRFWNN uncertainty observer and $\mathcal{H}_\infty$ control methodology to control the rotor position of the PMSM servo drive considering the existence of load disturbances and parameters uncertainties.

REFERENCES

[1] W. Leonhard, Control of Electrical Drives, Springer-Verlag, Berlin, 1996.
[2] R. Krishnan, Electric Motor Drives: Modeling, Analysis, and Control, Prentice-Hall, New Jersey, 2001.
[3] F. F. M. El-Sousy, Robust Wavelet–Neural–Network Sliding–Mode Control System for Permanent-Magnet Synchronous Motor Drive, IET—Electric Power Application, Vol. 5, No. 1, 2011, pp. 113–132.
[4] K. Jezernik, M. Rodic, High Precision Motion Control of Servo Drives, IEEE Trans. on Industrial Electronics, Vol. 56, No. 10, 2009, pp. 3810-3816.
[5] J. W. Finch, D. Giaouris, Controlled AC Electrical Drives, IEEE Trans. on Industrial Electronics, Vol. 55, No. 2, 2008, pp. 481-491.
[6] Xuefang Lin-Shi, F. Morel, A.M. Llor, B. Allard, J.-M. Retif, Implementation of Hybrid Control for Motor Drives, IEEE Trans. on Industrial Electronics, Vol. 54, No. 4, 2007, pp. 1946-1952.
[7] I. Kanellakopoulos, P. V. Kokotovic and A. S. Morse, Systematic design of adaptive controller for feedback linearizable systems, IEEE Trans. Autom. Control, Vol. 36, No. 11, 1991, pp. 1241–1253.
[8] M. Krstic, I. Kanellakopoulos, and P. V. Kokotovic, Nonlinear and Adaptive Control Design. New York: Wiley, 1995.

[9] H. J. Shieh and K. K. Shyu, Nonlinear sliding-mode torque control with adaptive backstepping approach for induction motor drive, IEEE Trans. Ind. Electron., Vol. 46, No. 2, 1999, pp. 380–389.

[10] F. J. Lin and C. C. Lee, Adaptive backstepping control for linear induction motor drive to track periodic references, IEE Proc.—Electron. Power Appl., Vol. 147, No. 6, 2000, pp. 449–458.

[11] Y. Li, S. Qiang, X. Zhuang, and O. Kaynak, Robust and adaptive backstepping control for nonlinear systems using RBF neural networks, IEEE Trans. Neural Netw., Vol. 15, No. 3, 2004, pp. 693–701.

[12] T. Zhang, S. S. Ge, and C. C. Hang, Adaptive neural network control for strict-feedback nonlinear systems using backstepping design, Automatica, Vol. 36, 2000, pp. 1835–1846.

[13] J. Y. Choi and J. A. Farrell, Adaptive observer backstepping control using neural networks, IEEE Trans. Neural Netw., Vol. 12, No. 5, 2001, pp. 1103–1112.

[14] O. Kuljaca, N. Swamy, F.L. Lewis, and C.M. Kwan, Design and implementation of industrial neural network controller using backstepping, IEEE Trans. Ind. Electron., Vol. 50, No. 1, 2003, pp. 193–201.

[15] C. M. Lin and C. F. Hsu, Recurrent-neural-network-based adaptive backstepping control for induction servomotor, IEEE Trans. Ind. Electron., Vol. 52, No. 6, 2005, pp. 1677–1684.

[16] Chun-Fei Hsu, Chih-Min Lin and Tsu-Tian Lee, Wavelet Adaptive Backstepping Control for a Class of Nonlinear Systems, IEEE Trans. on Neural Netw., Vol. 17, No. 5, 2006, pp. 1175-1183.

[17] Faa-Jeng Lin, Po-Huang Shieh, and Po-Huan Chou, Robust Adaptive Backstepping Motion Control of Linear Ultrasonic Motors Using Fuzzy Neural Network, IEEE Trans. on Fuzzy Syst., Vol. 16, No. 3, 2008, pp. 676-692.

[18] Rong-Jong Wai and Han-Hsiang Chang, Backstepping Wavelet Neural Network Control for Indirect Field-Oriented Induction Motor Drive, IEEE Trans. on Neural Netw., Vol. 15, No. 2, 2004, pp. 367-383.

[19] C. M. Kwan and F. L. Lewis, Robust Backstepping Control of Induction Motors Using Neural Networks, IEEE Trans. on Neural Netw., Vol. 11, No. 5, 2000, pp. 1178-1187.

[20] Yaolong Tan, Jie Chang, and Hualin Tan, Adaptive Backstepping Control and Friction Compensation for AC Servo With Inertia and Load Uncertainties, IEEE Trans. Ind. Electron., Vol. 50, No. 5, 2003, pp. 944-952.

[21] R. J. Wai, Hybrid control for speed sensorless induction motor drive, IEEE Trans. Fuzzy Systems, Vol. 9, No. 1, 2001, pp. 116-138.

[22] K. S. Narendra and K. Parthasarathy, Identification and control of dynamical systems using neural networks, IEEE Trans. Neural Networks, Vol. 1, No. 1, 1990, pp. 4–27.

[23] Y. G. Leu, T. T. Lee and W. Y. Wang, On-line tuning of fuzzy-neural network for adaptive control of nonlinear dynamical systems, IEEE Trans. Syst., Man, Cybern., Vol. 27, No. 6, 1997, pp. 1034-1043.

[24] Y. M. Park, M. S. Choi, and K. Y. Lee, An optimal tracking neurocontroller for nonlinear dynamic systems, IEEE Trans. Neural Networks, Vol. 7, No. 5, 1996, pp. 1099–1110.

[25] K. T. Tanaka and H. O. Wang, Fuzzy Control Systems Design and Analysis, New York: Wiley, 2001.

[26] Y. S. Lu and J. S. Chen, A self-organizing fuzzy sliding-mode controller design for a class of nonlinear servo systems, IEEE Trans. Indust. Electron., Vol. 41, No. 5, 1994, pp. 492–502.

[27] F. J. Lin, W. J. Hwang, and R. J. Wai, A supervisory fuzzy neural network control system for tracking periodic inputs, IEEE Trans. Fuzzy Syst., Vol. 7, No. 1, 1999, pp. 41–52.

[28] W. Y. Wang, Y. G. Leu, and C. C. Hsu, Robust adaptive fuzzy-neural control of nonlinear dynamical systems using generalized projection update law and variable structure controller, IEEE Trans. Syst., Man, Cybern. B, Vol. 31, No. 1, 2001, pp. 140–147.

[29] C. H. Wang, H. L. Liu, and T. C. Lin, Direct adaptive fuzzy-neural control with state observer and supervisory controller for unknown nonlinear dynamical systems, IEEE Trans. Fuzzy Syst., Vol. 10, No. 1, 2002, pp. 39–49.

[30] Y. G. Leu, W. Y. Wang, and T. T. Lee, Robust adaptive fuzzy-neural controllers for uncertain nonlinear systems, IEEE Trans. Robot. Automat., Vol. 15, No. 5, 1999, pp. 805–817.

[31] J. Zhang and A. J. Morris, Recurrent neuro-fuzzy networks for nonlinear process modeling, IEEE Trans. Neural Networks, Vol. 10, No. 2, 1999, pp. 313–326.

[32] F. J. Lin and C. H. Lin, Online gain-tuning IP controller using RFNN, IEEE Trans. Aerosp. Electron. Syst., Vol. 37, No. 2, 2001, pp. 655–670.

[33] C. H. Lee and C.C. Teng, Identification and Control of Dynamic Systems Using Recurrent-Fuzzy-Neural-Network, IEEE Transaction on Fuzzy Systems, Vol. 8, No. 4, 2000, pp. 349-366.

[34] F. F. M. El-Sousy, Robust adaptive H∞ position control via a wavelet-neural-network for a DSP-based permanent-magnet synchronous motor servo drive system, IET—Electric Power Application, Vol. 4, No. 5, 2010, pp. 333–347.

[35] C. F. Hsu and K. H. Cheng, Recurrent Fuzzy-Neural approach for nonlinear control using dynamic structure learning scheme, Neurocomputing, Vol. 71, No. 16-18, 2008, pp. 3447-3459.

[36] F. F. M. El-Sousy, Robust Adaptive Wavelet-Neural-Network Sliding-Mode Control for a DSP-Based PMSM Drive System, Journal of Power Electronics, JPE, Vol. 10, No. 5, 2010, pp. 518-527.

[37] B. Delyon, A. Juditsky, and A. Benveniste, Accuracy analysis for wavelet approximations, IEEE Trans. on Neural Networks, Vol. 6, 1995, pp. 332–348.

[38] C. F. Chen and C. H. Hsiao, Wavelet approach to optimizing dynamic systems, Proc. IEE—Control Theory Application, Vol. 146, No. 2, 1999, pp. 213–219.

[39] Q. Zhang and A. Benveniste, Wavelet networks, IEEE Trans. on Neural Networks, Vol. 3, 1992, pp. 889–898.

[40] J. Zhang, G. G. Walter, Y. Miao, and W. N. W. Lee, Wavelet neural networks for function learning, IEEE Trans. on Signal Processing, Vol. 43, 1995, pp. 1485–1496.

[41] N. Sureshbabu and J. A. Farrell, Wavelet-based system identification for nonlinear control, IEEE Trans. on Automatic Control, Vol. 44, No. 2, 1999, pp. 412–417.

[42] S. A. Billings and H. L. Wei, A new class of wavelet networks for nonlinear system identification, IEEE Trans. on Neural Network, Vol. 16, No. 4, 2005, pp. 862–874.

[43] D. Giaouris, J.W. Finch, O.C. Ferreira, R.M. Kennel, G. M. El-Murr, Wavelet Denoising for Electric Drives, IEEE Trans. on Industrial Electronics, Vol. 55, No. 2, 2008, pp. 543–550.

[44] C.-H. Lu, "Design and Application of Stable Predictive Controller Using Recurrent Wavelet Neural Networks," IEEE Trans. on Industrial Electronics, Vol. 56, No. 9, pp. 3733-3742, Sept 2009.

[45] [45] D. Gonzalez, J.T. Bialasiewicz, J. Balcells, J. Gago, Wavelet-Based Performance Evaluation of Power Converters Operating With Modulated Switching Frequency, IEEE Trans. on Industrial Electronics, Vol. 55, No. 8, 2008, pp. 3167-3176.

[46] Kinjiro Yoshida, M. El-Nemr and F. F. M. El-Sousy, Propulsion and Levitation H∞ Optimal Control of Underwater Linear Motor Vehicle ME02, WSEAS Transactions on Systems, No. 7, Vol. 4, 2005, pp. 1009-1016.

[47] F. F. M. El-Sousy, Hybrid H∞–Based Wavelet-Neural-Network Tracking Control for Permanent-Magnet Synchronous Motor Drives, IEEE Trans. on Indust. Electronics, Vol. 57, No. 9, 2010, pp. 3157-3166.

[48] F. F. M. El-Sousy, Hybrid recurrent cerebellar model articulation controller-based supervisory H∞ motion control system for permanent-magnet synchronous motor servo drive, IET—Electric Power Application, Vol. 5, No. 7, 2011, pp. 563–579.

[49] F. F. M. El-Sousy, Robust adaptive H∞ position control via a wavelet-neural-network for a DSP-based permanent-magnet synchronous motor servo drive system, IET—Electric Power Application, Vol. 4, No. 5, 2010, pp. 333–347.

[50] Y. C. Chang and B. S. Chen, A nonlinear adaptive H∞ tracking control design in robotic systems via neural networks, IEEE Trans. on Control System Technology, Vol. 5, 1997, pp. 13–29.

[51] C. Attaianese, A. Perfetto, and G. Tomasso, Robust position control of DC drives by means of H∞ controllers, Proc. IEE—Electric Power Application, Vol. 146, No. 4, 1999, pp. 391–396.

[52] M. C. Hwang, X. Hu, and Y. Shrivastava, Adaptive H∞ neural network tracking controller for electrically driven manipulators, Proc. IEE—Control Theory Application, Vol. 145, No. 6, 1998, pp. 594–602.

[53] J. A. Ball, P. Kachroo, and A. J. Krener, H∞ tracking control for a class of nonlinear systems , IEEE Trans. on Automatic Control, Vol. 44, No. 6, 1999, pp. 1202–1206.

[54] S. Katayama, K. Yubai, J. Hirai, Iterative Design of the Reduced-Order Weight and Controller for the H∞ Loop-Shaping Method Under Open-

Loop Magnitude Constraints for SISO Systems, IEEE Trans. on Industrial Electronics, Vol. 56, No. 10, 2009, pp. 3854-3863.

[55] G. Willmann, D.F. Coutinho, L.F.A. Pereira, F.B. Libano, Multiple-Loop H-Infinity Control Design for Uninterruptible Power Supplies, IEEE Trans. on Ind. Electron., Vol. 54, No. 3, 2007, pp. 1591-1602.

[56] B. S. Chen and C. H. Lee, H∞ tracking design of uncertain nonlinear SISO systems: Adaptive fuzzy approach, IEEE Trans. Fuzzy Syst., Vol. 4, No. 1, 1996, pp. 32–43.

[57] W. Y. Wang, M. L. Chan, C. C. J. Hsu, and T. T. Lee, H∞ tracking-based sliding mode control for uncertain nonlinear systems via an adaptive fuzzy-neural approach, IEEE Trans. Syst., Man, Cybern. B, Cybern., Vol. 32, No. 4, 2002, pp. 483–492.

[58] C. L. Lin and T. Y. Lin, Approach to adaptive neural net-based H∞ control design, Proc. IEE, Contr. Theory Appl., Vol. 149, No. 4, 2002, pp. 331–342.

[59] [59]   D. W. C. Ho, P. A. Zhang, and J. Xu, Fuzzy wavelet networks for function learning, IEEE Trans. Fuzzy Syst., Vol. 9, No. 1, 2001, pp. 200–211.

[60] R. H. Abiyev, O. Kaynak, Fuzzy Wavelet Neural Networks for Identification and Control of Dynamic Plants—A Novel Structure and a Comparative Study, IEEE Trans. on Industrial Electronics, Vol. 55, No. 8, 2008, pp. 3133-3140.

[61] S. Yilmaz and Y. Oysal, Fuzzy wavelet neural network models for prediction and identification of dynamical systems, IEEE Trans. Neural Netw., Vol. 21, No. 10, 2010, pp. 1599–1609.

[62] CH Lu, Wavelet fuzzy neural networks model for identification and predictive control of dynamical systems, IEEE Trans. Ind. Electron., Vol. 58, No. 7, 2011, pp. 3046–3058.

[63] C. F. Hsu, Adaptive fuzzy wavelet neural controller design for chaos synchronization, Expert. Syst. with Appli. an International Journal, Vol. 38, No. 810483, 2011, pp. 10475–.

[64] M. Davanipoor M. Zekri and F. Sheikholeslam, Fuzzy wavelet neural network with an accelerated hybrid learning algorithm, IEEE Trans. Fuzzy Syst., Vol. 20, No. 3, 2012, pp. 463–470.

[65] Smriti Srivastava, Madhusudan Singh, M. Hanmandlu and A.N. Jha, New fuzzy wavelet neural networks for system identification and control, Applied Soft Computing, Vol. 6, No. 1, 2005, pp. 1–17.

[66] Shian-Tang Tzeng, Design of fuzzy wavelet neural networks using the GA approach for function approximation and system identification, Fuzzy Sets and Systems, Vol. 161, No. 19, 2010, pp. 2585–2596.

[67] Y. Bodyanskiy and O. Vynokurova, Hybrid adaptive wavelet-neuro-fuzzy system for chaotic time series identification, Information Sciences, Vol. 220, No. 20, 2013, pp. 170–179.

[68] M. Zekri, S. Sadri, and F. Sheikholeslam Adaptive fuzzy wavelet network control design for nonlinear systems, Fuzzy Sets Syst., Vol. 159, No. 20, 2008, pp. 2668–2695.

[69] F. F. M. El-Sousy, Robust Recurrent Wavelet Interval Type-2 Fuzzy-Neural-Network Control for a DSP-Based PMSM Servo Drive System", J. of Power Electronics (JPE), Vol. 13, No. 1, 2013, pp. 139-160.

[70] F. F. M. El-Sousy, Intelligent Optimal Recurrent Wavelet Elman Neural Network Control System for Permanent-Magnet Synchronous Motor Servo Drive, IEEE Trans. on Ind. Informatics, Vol. 9, No. 4, 2013, pp. 1986 –2003.

[71] J. Rodriguez, R.M. Kennel, J.R. Espinoza, M. Trincado, C.A. Silva, C.A. Rojas, High-Performance Control Strategies for Electrical Drives: An Experimental Assessment, IEEE Trans. on Ind. Electronics, Vol. 59, No. 2, 2012, pp. 812-820.

[72] R. Errouissi, M. Ouhrouche, Wen-Hua Chen, A.M. Trzynadlowski, Robust Cascaded Nonlinear Predictive Control of a Permanent Magnet Synchronous Motor With Antiwindup Compensator, IEEE Trans. on Ind. Electronics, Vol. 59, No. 8, 2012, pp. 3078-3088.

[73] Han Ho Choi, Nga Thi-Tuy Vu, Jin-Woo Jung, Design and Implementation of a Takagi–Sugeno Fuzzy Speed Regulator for a Permanent Magnet Synchronous Motor, IEEE Trans. on Ind. Electronics, Vol. 59, No. 8, 2012, pp. 3069-3077.

[74] R. Errouissi, M. Ouhrouche, Wen-Hua Chen, A.M. Trzynadlowski, Robust Nonlinear Predictive Controller for Permanent-Magnet Synchronous Motors With an Optimized Cost Function, IEEE Trans. on Ind. Electronics, Vol. 59, No. 7, 2012, pp. 2849-2858.

[75] H. Chaoui, P. Sicard, Adaptive Fuzzy Logic Control of Permanent Magnet Synchronous Machines With Nonlinear Friction, IEEE Trans. on Ind. Electronics, Vol. 59, No. 2, 2012, pp. 1123-1133.

[76] J.J.E. Slotine and W. LI, Applied Nonlinear Control, Prentice-Hall, New Jersey, 1991.

[77] K.J. Astrom and B. Wittenmark, Adaptive Control, Addison-Wesley, New York, 1995.